

Understanding the Reactivity and Decomposition of a Highly Active Iron Pincer Catalyst for Hydrogenation and Dehydrogenation Reactions

J. B. Curley, M. Z. Ertem

To be published in "ACS CATALYSIS"

August 2021

Chemistry Department
Brookhaven National Laboratory

U.S. Department of Energy
USDOE Office of Science (SC), Basic Energy Sciences (BES) (SC-22)

Notice: This manuscript has been authored by employees of Brookhaven Science Associates, LLC under Contract No. DE-SC0012704 with the U.S. Department of Energy. The publisher by accepting the manuscript for publication acknowledges that the United States Government retains a non-exclusive, paid-up, irrevocable, world-wide license to publish or reproduce the published form of this manuscript, or allow others to do so, for United States Government purposes.

DISCLAIMER

This report was prepared as an account of work sponsored by an agency of the United States Government. Neither the United States Government nor any agency thereof, nor any of their employees, nor any of their contractors, subcontractors, or their employees, makes any warranty, express or implied, or assumes any legal liability or responsibility for the accuracy, completeness, or any third party's use or the results of such use of any information, apparatus, product, or process disclosed, or represents that its use would not infringe privately owned rights. Reference herein to any specific commercial product, process, or service by trade name, trademark, manufacturer, or otherwise, does not necessarily constitute or imply its endorsement, recommendation, or favoring by the United States Government or any agency thereof or its contractors or subcontractors. The views and opinions of authors expressed herein do not necessarily state or reflect those of the United States Government or any agency thereof.

Understanding the Reactivity and Decomposition of a Highly Active Iron Pincer Catalyst for Hydrogenation and Dehydrogenation Reactions

Julia B. Curley,^{a,†} Nicholas E. Smith,^{a,†} Wesley H. Bernskoetter,^b Mehmed Z. Ertem,^c Nilay Hazari,^{a,*} Brandon Q. Mercado,^a Tanya M. Townsend,^a and Xiaoping Wang^d

^aThe Department of Chemistry, Yale University, P. O. Box 208107, New Haven, Connecticut, 06520, USA. E-mail: nilay.hazari@yale.edu.

^bThe Department of Chemistry, The University of Missouri, Columbia, Missouri, 65211, USA.

^cChemistry Division, Brookhaven National Laboratory, Upton, New York 11973-5000, USA.

^dNeutron Scattering Division, Oak Ridge National Laboratory, Oak Ridge, Tennessee 37831, USA.

[†]Denotes that the authors made equal contribution.

Abstract

The iron pincer complex (ⁱPrPNP)Fe(H)(CO) (**1**, ⁱPrPNP⁻ = N(CH₂CH₂PⁱPr₂)₂⁻) is an active (pre)catalyst for many hydrogenation and dehydrogenation reactions. This is in part because **1** can reversibly add H₂ across the iron-amide bond to form (ⁱPrPN^HP)Fe(H)₂(CO) (**2**, ⁱPrPN^HP = HN(CH₂CH₂PⁱPr₂)₂). However, rapid decomposition limits the catalytic performance of **1** and related complexes. We explored the pathways through which catalytic intermediates related to **1** and **2** undergo decomposition. This involved characterizing the unstable and previously unobserved complexes [(ⁱPrPN^HP)Fe(H)(CO)(L)]⁺ (**5-L**; L = THF or N₂) and [(ⁱPrPN^HP)Fe(H)(H₂)(CO)]⁺ (**8**), which are proposed as intermediates when **1** and **2** are used as catalysts. Compound **8** was synthesized through the reaction of (ⁱPrPN^HP)Fe(H)(CO)(PF₆) (**6**) with H₂, and the solid-state structure was established using both X-ray and neutron diffraction. As part of our studies understanding the reactivity of **5-L**, we determined the thermodynamic hydricity of **2**, which is valuable for predicting its reactivity as a hydride donor. Further, it is shown that species such as **5-L** decompose to the same inactive species observed in catalysis using **1** and **2**, and theoretical calculations suggest that this likely occurs via a bimolecular pathway. To provide support for this hypothesis we isolated the dimeric species [{(ⁱPrPN^HP)Fe(H)(CO)}₂{μ-CN}]⁺ (**11**) and [{(ⁱPrPN^HP)Fe(H)(CO)}₂{μ-OC(H)O}]⁺ (**12**), which indicates that catalytic intermediates ligated by ⁱPrPN^HP can form dimeric species. Our results provide general strategies for improving catalysis using **1** and **2**, and we used this information to rationally increase the performance of **1** in formic acid dehydrogenation.

Introduction

The development of ligands capable of participating in reactions involving metal-ligand cooperation (MLC)¹ has led to highly active and productive pincer supported catalysts for the hydrogenation and dehydrogenation ((de)hydrogenation) of polar substrates.² In particular, ruthenium and iridium catalysts supported by pincer ligands that can add or eliminate H₂ via pathways based on MLC are used for the hydrogenation of a plethora of substrates including ketones,³ aldehydes,³ nitriles,⁴ esters,⁵ unsaturated N-heterocycles,⁶ and CO₂.⁷ Notably, the Ru-MACHO catalyst, (P^hPN^HP)Ru(H)(Cl)(CO) (P^hPN^HP = HN(CH₂CH₂PPh₂)₂), is commercially utilized for the hydrogenation of bio-derived methyl lactate to 1,2-propanediol.⁸ In many cases, the same systems are also excellent catalysts for the microscopic reverse dehydrogenation reactions such as the conversion of alcohols to ester and ketones.⁹ There is, however, a drive to replace precious metal catalysts with systems based on first-row transition metals due to their increased abundance and generally lower cost and toxicity.^{10,11}

Complexes derived from (iPrPNP)Fe(H)(CO) (**1**, iPrPNP = N(CH₂CH₂PⁱPr₂)₂), which is capable of reversibly activating H₂ to form (iPrPN^HP)Fe(H)₂(CO) (**2**, iPrPN^HP = HN(CH₂CH₂PⁱPr₂)₂) (Figure 1), have recently been utilized as catalysts for a variety of (de)hydrogenation reactions.¹² For example, **1** and its derivatives (such as **2**) are active catalysts for the hydrogenation of esters,¹³ ketones,^{13a} nitriles,¹⁴ amides,¹⁵ N-heterocycles,¹⁶ olefins,¹⁷ and the conversion of CO₂ to formate.¹⁸ They are also utilized for the dehydrogenation of formic acid,¹⁹ primary and secondary alcohols,^{13a,20} polyols such as glycerol,²¹ N-heterocycles,¹⁶ and ammonia-borane,²² and can mediate the dehydrogenative synthesis of lactones,²³ lactams,²³ amides,²⁴ and ureas.²⁵ In general, the turnover frequencies and turnover numbers (TONs) of **1** and its derivatives are lower than those observed with related second- and third-row transition metal catalysts, due in part to faster decomposition of the first-row transition metal based systems.²⁶

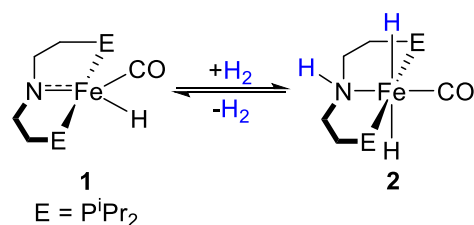


Figure 1: Activation of H₂ via a MLC pathway by iron catalysts for the (de)hydrogenation of polar substrates.

There are currently a paucity of studies investigating the pathways for decomposition of **1** or related first-row systems in (de)hydrogenation reactions, despite rapid catalyst deactivation being

a major limitation in catalyst performance.^{20,26} The dicarbonyl complexes (*i*PrPN^HP)Fe(CO)₂ (**3**) and [(*i*PrPN^HP)Fe(H)(CO)₂]⁺ (**4**, Figure 2) have been identified as decomposition products in catalysis using **1**, but there is no insight into how they are formed.^{13a,18-19,20b} Additionally, the formation of **3** and **4** in different catalytic reactions under different conditions suggests that the second carbonyl ligand is not formed from reaction components such as solvent or substrate. As a result, the presence of two CO ligands bound to iron in **3** and **4** implies that the decomposition process consumes two equivalents of the catalyst. Further, catalytic studies demonstrate that lower TONs occur at higher catalyst loadings and concentrations, which also implies that the decomposition process may be bimolecular.^{13a} However, there is only one example of a dimeric iron complex with the *i*PrPN^HP ligand,²⁷ and this contains a bridging BH₄⁻ ligand, which is not relevant to the vast majority of catalytic (de)hydrogenation reactions.²²

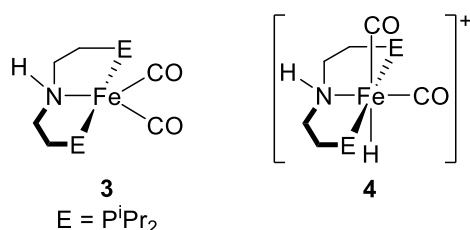


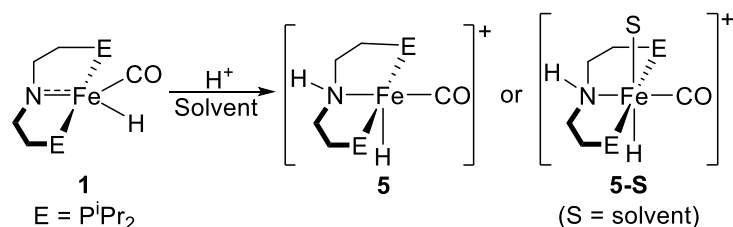
Figure 2: Previously observed decomposition products, which are proposed to form via a bimolecular pathway, in the catalytic (de)hydrogenation of polar substrates using **1** and derivatives. An equivalent of free ligand is also observed upon the formation of **3** or **4**.

Herein, we present an experimental study, supported by theoretical calculations, of the properties and deactivation of catalytic intermediates related to **1** and its derivatives. Specifically, we have synthesized and characterized several previously unobserved catalytic intermediates, such as the solvento complex [(*i*PrPN^HP)Fe(H)(CO)(solv)]⁺ (solv = THF or Et₂O) and the molecular H₂ complex [(*i*PrPN^HP)Fe(H)(CO)(H₂)]⁺, which are highly unstable and decompose readily. This provides information about the stability and reactivity of different catalytic intermediates derived from **1** and includes a determination of the thermodynamic hydricity of **2**. Further, we have demonstrated that catalytic intermediates supported by the *i*PrPN^HP ligand can form dimeric species, such as a complex with a bridging formate ligand. This suggests that the dimerization of two catalyst molecules is a plausible decomposition route in catalysis. We use these results to develop guidelines on how to increase catalyst lifetime, which should be beneficial for modifying reaction conditions and designing new catalysts with improved TONs. We have demonstrated this approach by rationally modifying the reaction conditions to generate an improved system for formic acid dehydrogenation based on **1**.

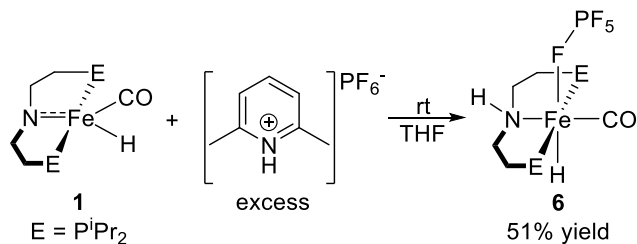
Results and Discussion

Protonation of 1 to Generate a Coordinatively Unsaturated Complex

Multiple catalytic reactions involving **1** include acidic species, such as carboxylic acids, alcohols or η^2 -dihydrogen iron complexes, as reaction components.^{13,15,19-21} As a result, the solvento complex $[(iPrPN^H P)Fe(H)(CO)(solv)]^+$ (**5-S**) or the related 16-electron cationic complex $[(iPrPN^H P)Fe(H)(CO)]^+$ (**5**) are proposed as catalytic intermediates which could form through protonation of **1** (Scheme 1).^{19,20b} Nevertheless, these species have not previously been observed or spectroscopically characterized. We hypothesized that protonation of **1** with an acid containing a non-coordinating anion could result in the formation of **5-S** (Scheme 1). Initially, however, synthesis of **5-S** proved challenging. Protonation of **1** with 2,6-lutidinium hexafluorophosphate in THF (Scheme 2) led to a rapid reaction and the appearance of signals in the 1H NMR and IR spectra consistent with the formation of a complex with a protonated $iPrPN^H P$ ligand. To our surprise, the product was soluble in aromatic solvents such as benzene and toluene, suggesting that it is not a salt with an outer-sphere PF_6 anion. Instead, we propose that the product is the neutral complex $(iPrPN^H P)Fe(H)(CO)(PF_6)$ (**6**), where the PF_6 anion forms a contact ion pair with the cationic metal center, although single crystals of **6** could not be obtained. Several examples of complexes with a similarly coordinated PF_6 ligand are known in the literature.²⁸ The coordination of PF_6 to iron in **6** is supported by the ^{19}F and ^{31}P NMR spectra. The ^{19}F spectrum in C_6D_6 contains one broad peak at -76 ppm at both ambient temperature and -35 °C, consistent with a dynamic process in which the fluorine atom of the PF_6 anion that is coordinated to iron exchanges with an uncoordinated fluorine atom, presumably through a rapid rotation of the PF_6 anion. This behavior is in agreement with the NMR spectra of other complexes containing a bound PF_6 anion.²⁹ Additionally, instead of the characteristic septet for the PF_6 anion in the ^{31}P NMR spectrum, only a broad feature at -136 ppm is observed at ambient temperature. Density functional theory (DFT) calculations at M06 level of theory indicate that **6** is approximately 3 kcal/mol more favorable in



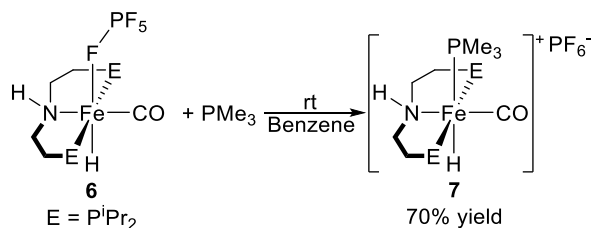
Scheme 1: Previously proposed but unobserved catalytic intermediates in catalytic (de)hydrogenation reactions facilitated by **1** and its derivatives.



Scheme 2: Synthesis of $[(iPrPN^H)Fe(H)(CO)(PF_6)]$ (**6**) from **1** and 2,6-lutidinium hexafluorophosphate.

a THF solution than $[(iPrPN^H)Fe(H)(CO)(THF)]^+$ with an outer-sphere PF_6^- . Although **6** is not a solvento complex, the relatively weak coordination of the PF_6^- anion, as determined by DFT calculations, suggests that its reactivity is likely to be analogous to **5** or **5-S**.

To support the hypothesis that the PF_6^- ligand of **6** can be readily displaced, we explored the reactivity of **6** with PMe_3 (Scheme 3). Addition of 1 equiv. of PMe_3 to a solution of **6** in benzene results in the formation of a precipitate, indicating that the product may have dissociated the PF_6^- anion to form a salt. The 1H NMR spectrum of the precipitate in $THF-d_8$ contains a new doublet of triplets at -12.0 ppm. In the ^{31}P NMR spectrum a new doublet at 91.5 ppm is assigned to the



Scheme 3: Synthesis of $[(iPrPN^H)Fe(H)(CO)(PMe_3)]^+$ (**7**).

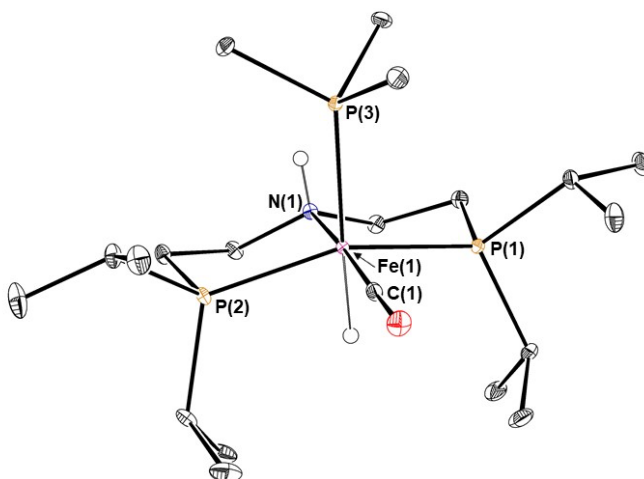
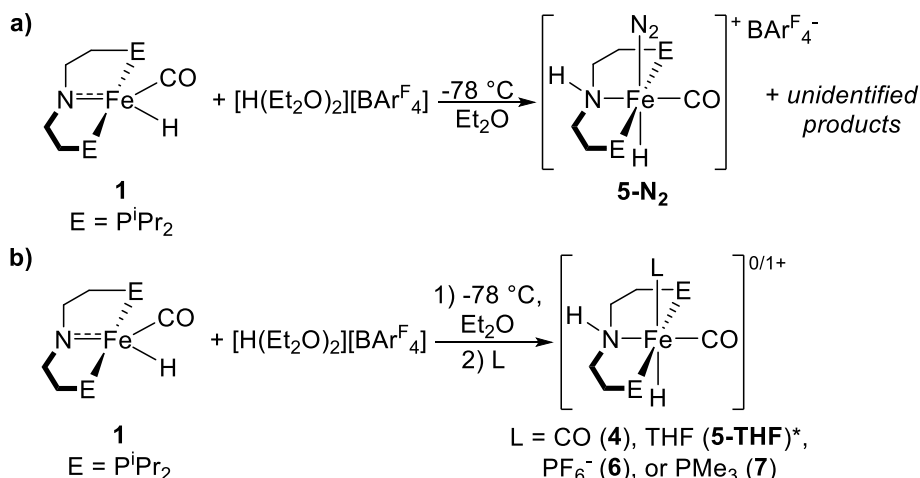


Figure 3: ORTEP of **7** with ellipsoids at 30% probability. The PF_6^- anion, hydrogen atoms not bound to Fe or N, and solvent of crystallization are excluded for clarity. Bond distances (Å) and angles (°): Fe(1)-N(1) 2.1032(18), Fe(1)-C(1) 1.727(2), Fe(1)-P(1) 2.2212(6), Fe(1)-P(2) 2.2263(6), Fe(1)-P(3) 2.2771(6); P(1)-Fe(1)-P(2) 155.79(3).

$i\text{PrPN}^{\text{H}}\text{P}$ ligand, while a triplet at -1.2 ppm is assigned to a coordinated PMe_3 ligand. This is consistent with PMe_3 binding and displacing PF_6 to produce the new complex $[(i\text{PrPN}^{\text{H}}\text{P})\text{Fe}(\text{H})(\text{CO})(\text{PMe}_3)]^+$ (**7**) with an outer-sphere PF_6 anion, which gives a diagnostic sharp septet at -144 ppm in the ^{31}P NMR spectrum. The structure of **7** was confirmed using X-ray crystallography (Figure 3). The geometry about the iron atom is distorted octahedral, with the $i\text{PrPN}^{\text{H}}\text{P}$ ligand forming a P-Fe-P bond angle of $155.79(3)^\circ$. The iron center lies 0.459 \AA above the P-N-P plane (above being considered the direction *syn* with the N-H of the pincer), which is likely due to steric repulsion between the PMe_3 and pincer ligand. This contrasts to the dichloride complex $(i\text{PrPN}^{\text{H}}\text{P})\text{Fe}(\text{Cl})_2(\text{CO})$, where the iron atom lies within 0.03 \AA of the P-N-P plane, and the hydridochloride complex $(i\text{PrPN}^{\text{H}}\text{P})\text{Fe}(\text{H})(\text{Cl})(\text{CO})$, where the iron atom lies 0.231 \AA above the P-N-P plane.²⁷ ^1H and ^{31}P NMR spectroscopy indicate that only one isomer of **7** is present in solution. On the basis of ^1H NOESY NMR spectroscopy, which indicates through-space coupling between the PMe_3 protons and the N-H moiety, we propose that the isomer observed in solution is the *syn* isomer. Overall, the facile substitution of PF_6 by PMe_3 in **6** indicates that the PF_6 ligand is labile.

Even though **6** can act as a synthetic analogue to **5-S**, we wanted to assess if **5-S** was synthetically accessible. We hypothesized that **1** needed to be protonated with an acid containing an even weaker coordinating anion than PF_6 . Protonation of **1** with either an excess of 2,6-lutidinium BAr^{F_4} ($\text{BAr}^{\text{F}_4} = \text{tetrakis}(3,5\text{-bis-trifluoromethyl(phenyl))borate}$) or 1 equiv. of Brookhart's acid,³⁰ $[\text{H}(\text{Et}_2\text{O})_2][\text{BAr}^{\text{F}_4}]$, in diethyl ether at $-78 \text{ }^\circ\text{C}$ under N_2 results in the generation of the same yellow solution (Scheme 4a). At ambient temperature, broad ^1H and ^{31}P NMR spectra are observed. Upon cooling to $-60 \text{ }^\circ\text{C}$, one major resonance is observed in the ^{31}P NMR spectrum with a corresponding resonance at -15.1 ppm in the ^1H NMR spectrum, suggesting that the major product contains an iron-hydride. Several other minor peaks are present in the ^{31}P NMR spectrum, indicating that the solution is a mixture of products (see SI). When the reaction mixture is subjected to three freeze-pump-thaw cycles and sealed under vacuum, the solution immediately changes color from bright yellow to green and there is a substantial decrease in the signal to noise in the ^1H and ^{31}P NMR spectra, along with the growth of several new resonances. Replacing the N_2 atmosphere leads to an immediate color change back to bright yellow and recovery of the original NMR spectra, which suggests that the primary species in solution has coordinated N_2 . In agreement with this hypothesis, a solution state IR spectrum taken of the mixture in C_6D_6 contains two strong absorption bands at



Scheme 4: Synthesis of **a**) **5-N₂** from **1** and [H(OEt₂)₂][BAr^F₄], and **b**) [(ⁱPrPN^HP)Fe(H)(CO)(L)]^{0/1+} (L = CO (**4**), THF (**5-THF**)*, PF₆⁻ (**6**), or PMe₃ (**7**)) from **1**, [H(OEt₂)₂][BAr^F₄], and L. ***5-N₂** and some unidentified products are also formed in this reaction.

1960 and 1815 cm⁻¹, which computed frequencies indicate are probably combinations of the N≡N and C≡O vibrations.³¹ The complex speciation observed could arise in part because complexes with both N₂ and solvent coordinated are present, with multiple isomers of each possible.³² In agreement with this hypothesis, protonation of **1** with excess 2,6-lutidinium BAr^F₄ provided single crystals of the N₂-bound complex [(ⁱPrPN^HP)Fe(H)(CO)(N₂)]⁺ (**5-N₂**) suitable for X-ray diffraction after slow diffusion of pentane into a diethyl ether solution at -30 °C (Figure 4).³³ In **5-N₂**, the bound N₂ ligand is approximately linear (there are two molecules in the asymmetric unit and the Fe-N-N bond angles are 175.6(7)° and 178.6(9)°) and essentially unactivated, as the N–N distance

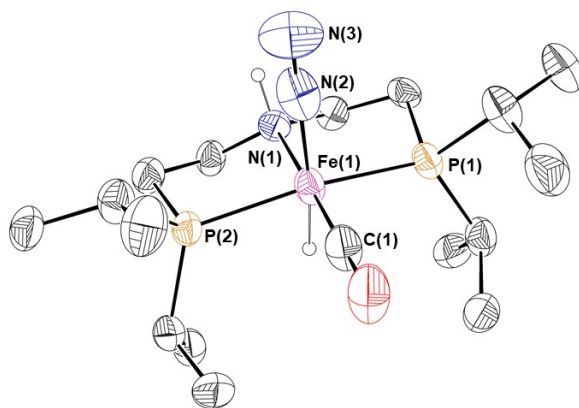


Figure 4: ORTEP of **5-N₂** with ellipsoids at 30% probability. The BAr^F₄ anion, hydrogen atoms not bound to Fe or N, disordered atoms, and solvent excluded for clarity. Two molecules are present in the asymmetric unit; only one is shown. Bond distances (Å) and angles (°) in the first molecule: Fe(1)-N(1) 2.074(7), Fe(1)-C(1) 1.744(10), Fe(1)-P(1) 2.230(2), Fe(1)-P(2) 2.201(6), Fe(1)-N(2) 1.904(8), N(2)-N(3) 1.101(8); P(1)-Fe(1)-P(2) 161.97(19), Fe(1)-N(2)-N(3) 175.6(7). In the second molecule: Fe(1)-N(1) 2.071(6), Fe(1)-C(1) 1.736(8), Fe(1)-P(1) 2.217(2), Fe(1)-P(2) 2.216(2), Fe(1)-N(2) 1.849(11), N(2)-N(3) 1.127(11); P(1)-Fe(1)-P(2) 162.97(10), Fe(1)-N(2)-N(3) 178.6(9).

(1.101(8) and 1.127(11) Å) is only slightly elongated compared to that of free N₂ (1.098 Å).³⁴ This is consistent with the observed N₂ bond lengths in other cationic iron(II) complexes with coordinated N₂.³⁴ Overall, the geometry about the iron center is best described as distorted octahedral, and the bond distances and angles around the iron are similar to the bis(carbonyl) analogue **4**.²⁷ In the crystal structure the N–H of the pincer ligand is *syn* to the N₂ ligand and hydrogen bonded to a diethyl ether solvent molecule, but likely in solution an isomer of **5-N₂** in which the N–H of the pincer ligand is *anti* to the N₂ ligand is also present (*vide infra*).

Protonation of **1** with Brookhart's acid in diethyl ether in the presence of more strongly coordinating ligands results in the clean formation of one product (Scheme 4b), supporting the hypothesis that **5-N₂** is formed in a mixture of products which all contain labile ligands in the sixth coordination site. For example, the addition of 1 equiv. of ⁿBu₄NPF₆ to a solution generated by protonating **1** with Brookhart's acid results in immediate effervescence and ¹H and ³¹P NMR spectra that match those of **6**. Similarly, addition of 1 atm of CO or 1 equivalent of PMe₃ to the reaction mixture results in the quantitative formation of the previously observed complexes [(ⁱPrPN^HP)Fe(H)(CO)₂]⁺ (**4**)²⁷ and [(ⁱPrPN^HP)Fe(H)(CO)(PMe₃)]⁺ (**7**), respectively. Interestingly, the addition of the relatively weakly binding THF to the reaction mixture from **1** and Brookhart's acid in diethyl ether, or removal of the diethyl ether *in vacuo* and dissolution of the crude solid in THF, results in the formation of an orange solution and immediate gas production. However, ¹H and ³¹P NMR spectra of the sample in THF are broad at ambient temperature and indicate complicated speciation. Upon cooling to 0 °C, four peaks are observed in the ³¹P NMR spectrum, with one corresponding to the decomposition product **4**. The predominant peak at 85.8 ppm is not present when the complex is dissolved in diethyl ether, suggesting that it is associated with a THF adduct. Further, there is a corresponding peak in the ¹H NMR spectrum at -29.1 ppm, consistent

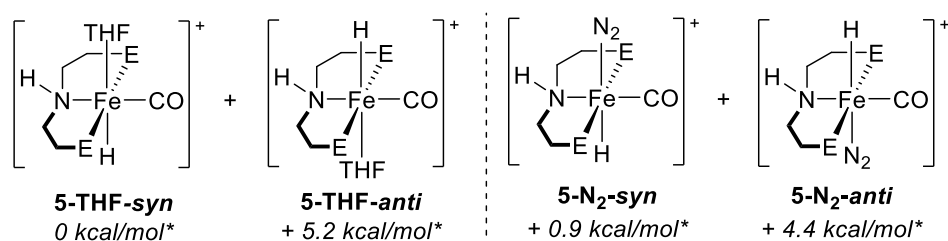
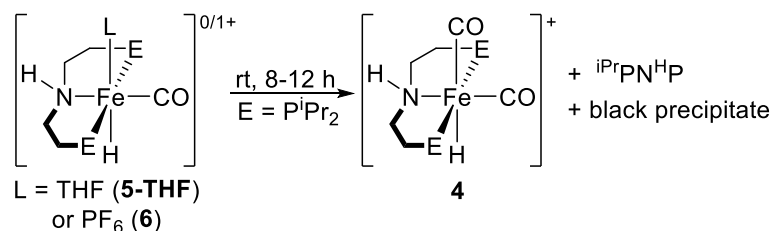


Figure 5: Relative energies of the isomers of **5-THF** and **5-N₂** as determined at M06 level of theory at 298 K. *The energy of **5-THF-syn** is set to 0 kcal/mol and the energies of **5-THF** include a molecule of free N₂ (at 1 atm), while the energies of **5-N₂** include a molecule of free THF. This allows comparison of the relative favorability of the isomers of **5-THF** versus **5-N₂**.

with a weak *trans*-influence ligand such as THF binding opposite the hydride.³⁵ The other two resonances present in the ³¹P NMR spectrum correspond with peaks observed when the mixture is dissolved in diethyl ether, and we propose that they are isomers of **5-N₂**. Overall, on the basis of observed changes to the reaction mixture upon the introduction of THF (including color, gas production, and NMR spectra) and the coordinating ability of THF,³⁶ we propose that one isomer of [(ⁱPrPN^HP)Fe(H)(CO)(THF)]⁺ (**5-THF**) is the predominant species in solution, with two isomers of [(ⁱPrPN^HP)Fe(H)(CO)(N₂)]⁺ (**5-N₂**) also present. The calculations suggest that the isomer of **5-THF** with the THF ligand *syn* to the N–H of the pincer ligand is the most thermodynamically favored at 298 K. Additionally, both isomers of **5-N₂** (N₂ ligand oriented *syn* or *anti* to N-H) are also thermally accessible if the errors associated with the calculations involving transition metal-based complexes with approximate density functionals and continuum solvation models are considered (Figure 5).³⁷ The *syn* isomer of **5-N₂** is more stable³⁷ than the *anti* isomer, consistent with our previous observations (*vide supra*).

Solutions of **5-THF** or **6** in THF (as well as benzene and toluene) are unstable and decompose completely within 8-12 hours (for a *ca.* 10 mM solution) upon standing at ambient temperature under either an N₂ or argon atmosphere. The decomposition products are **4** and the free ligand ⁱPrPN^HP in approximately a 1:1 ratio, as well as an unidentified precipitate which likely contains particulate iron(0) (Scheme 5). These products are identical to the decomposition products observed in the catalytic dehydrogenation of formic acid,^{19,38} which suggests that **5-THF** and related complexes undergo the same reactions involved in catalyst death.



Scheme 5: Decomposition of **5-THF** and **6**.

Although complexes of the type **5-S** may be potential intermediates in catalytic (de)hydrogenation reactions using derivatives of **1**, we propose that **5-N₂** is unlikely to be relevant in catalysis. This is because catalysis is generally conducted either a) at elevated temperatures, where the binding of N₂ is even less favorable than at room temperature due to entropic effects, or b) in the presence of H₂ (for hydrogenation reactions), which is a better ligand than N₂ (*vide infra*). As a result, we

chemical exchange between the bound H₂ ligand and the N–H of the pincer ligand or the Fe–H site. At room temperature and 1 atm of H₂, **8** is in equilibrium with **5-THF**, with the complexes being present in an approximately 2:1 ratio. Subjecting a THF solution of **8** to three freeze-pump-thaw cycles results in the complete regeneration of **5-THF**. Nevertheless, the equilibrium mixture is quite stable under an atmosphere of H₂, with a solution of the complexes showing only 20% decomposition to **4** over 10 days at room temperature. This suggests that decomposition via the formation of complexes with a very weakly bound ligand, such as **5-S**, is more likely to be a problem in dehydrogenation reactions rather than hydrogenation reactions performed with overpressures of H₂. Complex **8** is the first example of a spectroscopically characterized dihydrogen complex for a catalyst that is proposed to operate via a Noyori-type mechanism for hydrogenation, but two related iron dihydrogen complexes with pincer ligands that do not operate in MLC were recently reported.⁴⁰

In agreement with our observations from the reaction between **5-THF** and H₂, ¹H and ³¹P NMR spectroscopy indicates that the addition of 1 atm of H₂ to a solution of **6** in C₆D₆ results in spectra consistent with the formation of **8**, but with an outer-sphere PF₆ anion replacing the BAR^F₄ anion. In this case, at room temperature and 1 atm of H₂, only **8** is observed by ¹H NMR spectroscopy, with no evidence of an equilibrium between **8** and **6**. Over several days, single crystals of [(ⁱPrPN^HP)Fe(H)(H₂)(CO)]⁺[PF₆]⁻ suitable for X-ray diffraction precipitated from solution (Figure

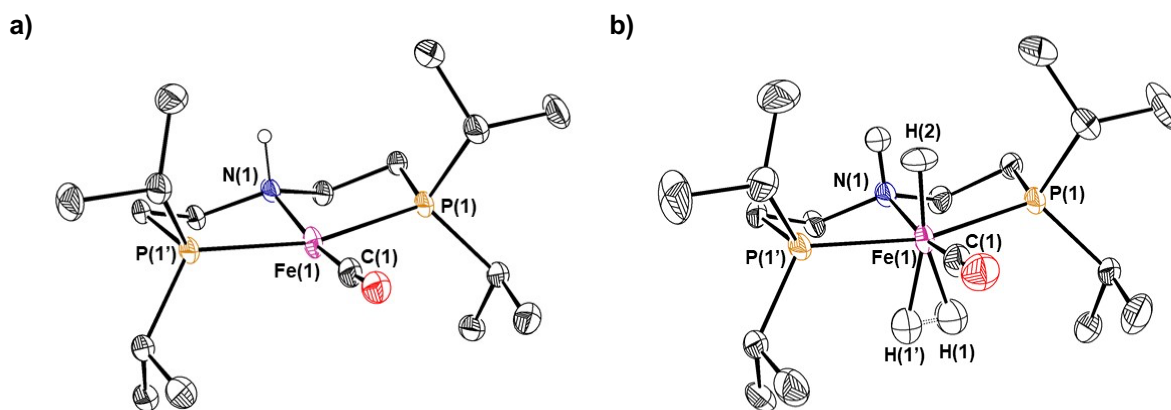


Figure 6: **a)** ORTEP of **8** as determined by X-ray diffraction. The PF₆ anion, hydrogen atoms not bound to N, and solvent of crystallization excluded for clarity. The molecule contains a mirror plane: Bond distances (Å) and angles (°): Fe(1)–N(1) 2.063(5), Fe(1)–C(1) 1.716(6), Fe(1)–P(1) 2.2135(9); P(1)–Fe(1)–P(1') 164.90(7). **b)** Solid-state structure of **8** as determined by Laue neutron diffraction. The PF₆ anion, selected hydrogen atoms, and solvent of crystallization are omitted for clarity. The molecule contains a mirror plane: Bond distances (Å) and angles (°): Fe(1)–H(1) 1.653(13), Fe(1)–H(2) 1.491(15), H(1)–H(1') 0.838(19); H(2)–Fe(1)–H(1) 165.3(3), H(1)–Fe(1)–H(1') 29.4(7). Both figures have ellipsoids at 30% probability.

6a).⁴¹ Although the hydride and molecular hydrogen ligands were not located in the Fourier map, the geometrical parameters associated with the pincer and CO ligands are similar to those observed in related ⁱPrPN^HP supported iron complexes and suggest an octahedral geometry around iron.²⁷ In order to gain more information about the solid-state structure of **8**, single crystals suitable for neutron diffraction were obtained. The single-crystal neutron diffraction derived model of **8** is shown in Figure 6b, and provides unambiguous confirmation that **8** contains both molecular hydrogen and hydride ligands. The geometric parameters associated with the non-hydrogen ligands are the same within error as those observed by X-ray diffraction, as expected. The neutron structure confirms that the H₂ ligand is *trans* to the hydride ligand. However, unlike in solution, the H₂ ligand is exclusively *anti* to the N–H of the pincer ligand, likely due to the presence of a hydrogen bonding interaction in the solid-state between the PF₆ anion and the N–H moiety (the shortest contact between the N–H and the PF₆ anion is 2.355(17) Å). The Fe–H bond distance associated with the classical hydride is 1.491(15) Å, while the bond lengths between the Fe and each of the hydrogen atoms associated with the H₂ ligand are 1.653(13) Å (the distances are the same due to symmetry). The H–H bond distance in the coordinated H₂ ligand is 0.838(19) Å, which matches with the distance determined using ¹H NMR spectroscopy (*vide supra*) and suggests only weak activation of H₂. These distances are consistent with those observed in the only two other iron complexes with molecular hydrogen ligands that have been characterized by neutron diffraction,⁴² which exclusively contain mono- and bi-dentate phosphine ligands. Further, this confirms that the estimation of the H–H bond distance from measurements of *T*₁(min) were not affected by the presence of an adjacent secondary amine ligand.

Decomposition Mechanisms via Transfer of a CO Ligand to 5-S

Our results regarding the synthesis and stability of **5-THF** and **6** suggest that dissociation of a THF or PF₆ ligand, respectively, to generate a 16e⁻ complex with a vacant coordination site is facile. Further, stoichiometric experiments demonstrate that the decomposition of **5-THF** and **6** generate the same deactivation species that are observed in catalysis, suggesting that species of this type are entry points for catalyst death. During catalysis, the decomposition of **5** to form **4** and an equivalent of free ligand likely occurs via the transfer of a CO ligand to **5** from an iron-containing intermediate, which could be another equivalent of **5** itself or a different species. However, our experimental results provide almost no information about the pathway for this process. Therefore,

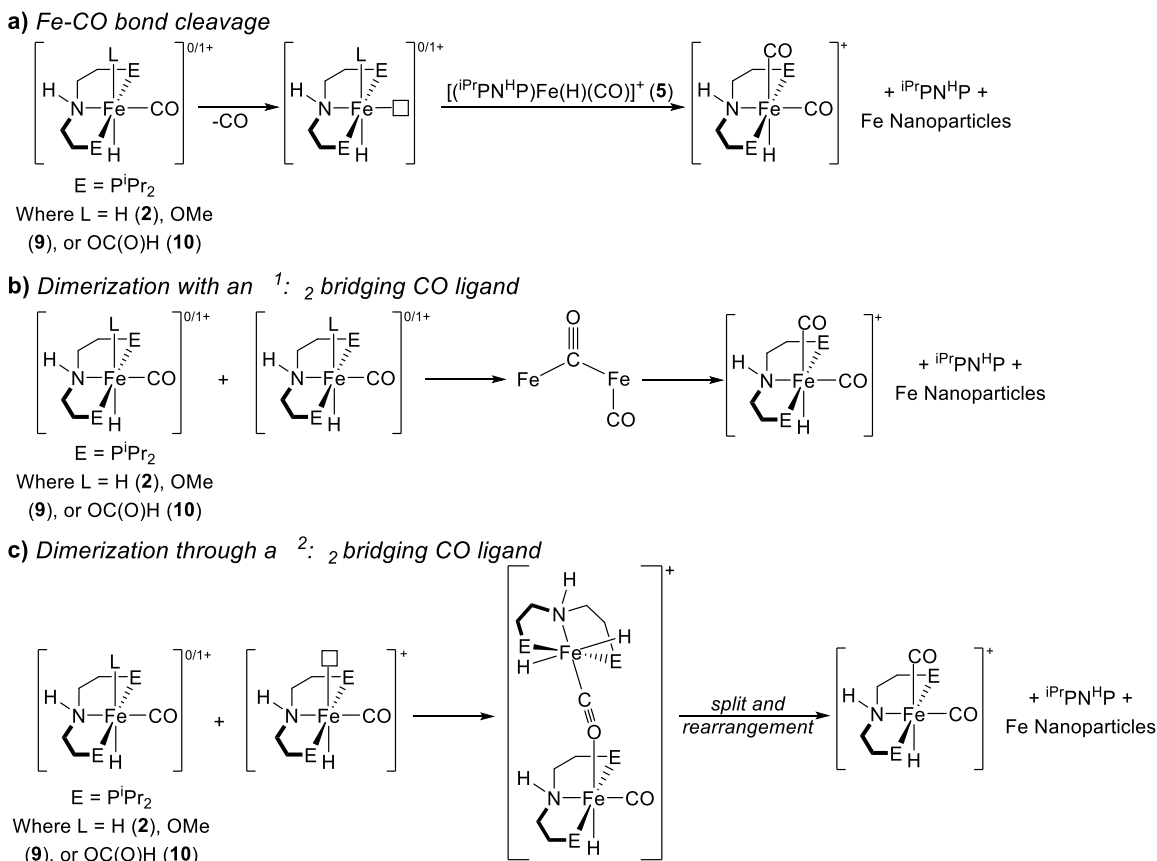


Figure 7: Potential mechanisms of CO transfer between iron centers for catalyst decomposition.

we used DFT calculations to assess several possibilities for CO transfer to **5** from other proposed catalytic intermediates such as **1**, **2**, **5-S**, and **6**. Two additional species are commonly formed in catalysis with **1** and derivatives. The first is the 1,2-addition product of an alcohol, such as MeOH, to **1** to form $(iPrPNHPr)Fe(H)(CO)(OCH_3)$ (**9**) (Figure 7).^{13a,20b} This is relevant to alcohol dehydrogenation and ester/ketone/aldehyde hydrogenation. The second is the formate complex $(iPrPNHPr)Fe(H)(CO)\{OC(O)H\}$ (**10**), relevant to formic acid¹⁹ and methanol^{20b} dehydrogenation as well as CO₂ hydrogenation.¹⁸ Pathways for CO transfer that were modelled include: a) Dissociative Fe–C bond cleavage from an iron-containing intermediate to form free CO, followed by binding of the free CO to **5**. b) The formation of a dimeric complex between **5** and another iron-containing species with a κ^1 -bridging CO ligand,⁴³ followed by rearrangement. c) The formation of a dimeric complex between **5** and another iron-containing species with an asymmetric end-on bridging CO ligand followed by rearrangement.⁴⁴

The cleavage of an Fe–CO bond, shown in Figure 7a, is not straightforward to calculate using DFT calculations because the products are likely to exist in either triplet or quintet states, and the

energies are highly dependent on the approximate DFT functional that is used (see SI). However, calculations at DLPNO-CCSD(T₁) level of theory on CO dissociation from **5-THF** and experimental studies on the rate of exchange of ¹³CO into [(ⁱPrPN^HP)Fe(CO)₂H]⁺ (**4**), a stable compound that is more likely to undergo CO loss than any catalytic intermediate, suggest that CO dissociation does not occur on the time scale of catalyst decomposition (see SI). Thus, it is unlikely to be a plausible pathway for the decomposition of catalytic intermediates. Additionally, despite repeated attempts, all structures involving a κ¹-binding mode of the CO ligand between coordinatively unsaturated **5** and **1**, **2**, **5**, **9**, or **10** failed to converge. Steric repulsion between the isopropyl substituents of the ⁱPrPN^HP ligands appear to prevent single-atom bridging carbon atom

between the iron centers, suggesting that the pathway depicted in Figure 7b is also not operative. However, the result of electrophilic attack by **5** on the CO ligand of **2** (the pathway depicted in Figure 7c) to form a dimer with an asymmetric end-on bridging CO ligand was observed to be only *ca.* 17 kcal/mol higher in energy than the monomeric units (Figure 8a). Further, electrophilic attack by **5** on the CO ligand of other catalytic intermediates, such as the 1,2- addition complex **9** (Figure 8b) or the formate complex **10** (Figure 8c), resulted in dimers that were also accessible at ambient temperature. In fact, dimerization of **5** and **9** is only uphill by 4.5 kcal/mol.⁴⁵ These results suggest that dimerization is a thermodynamically viable pathway for the decomposition of catalytic intermediates related to **1** and the most likely of the proposed mechanisms. Additionally,

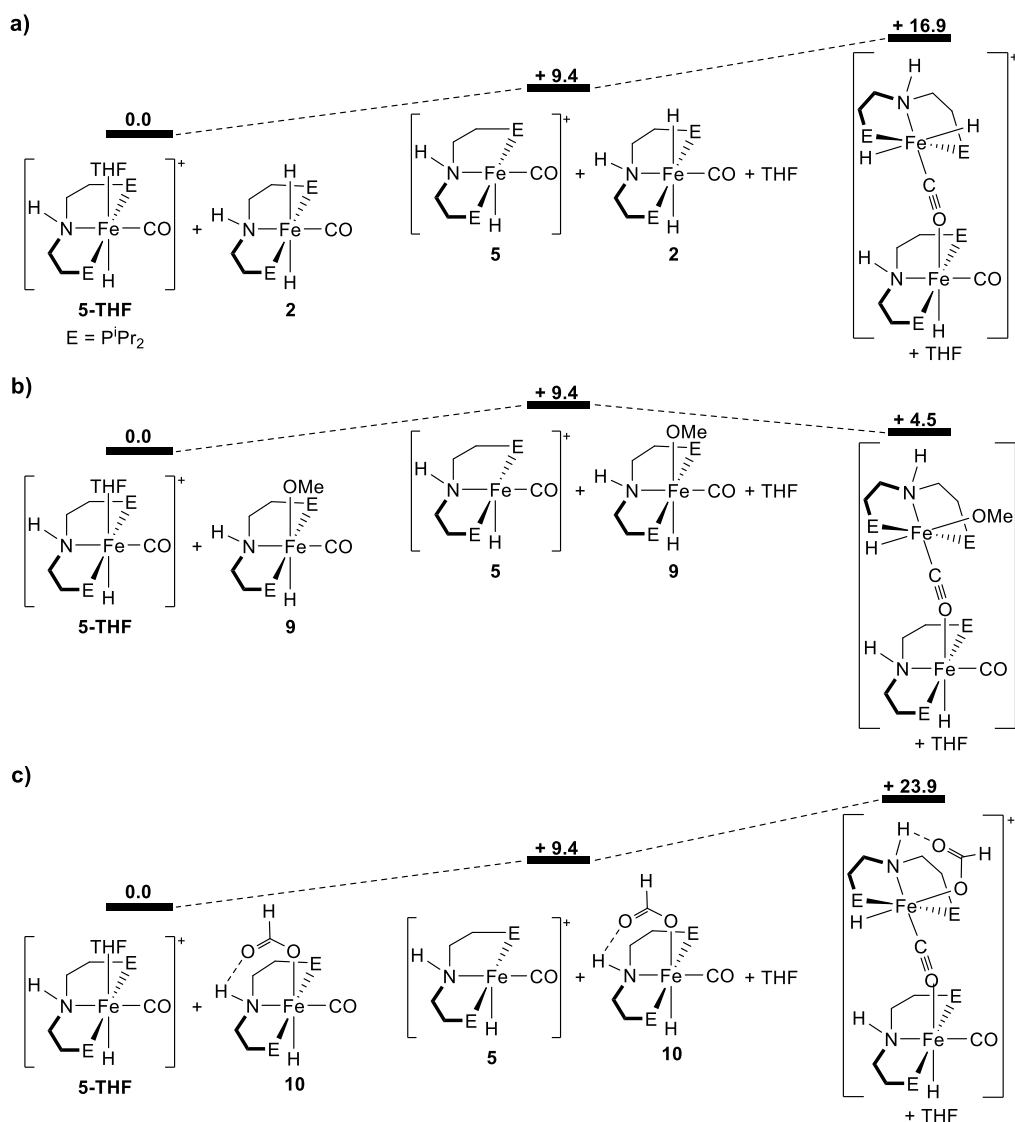
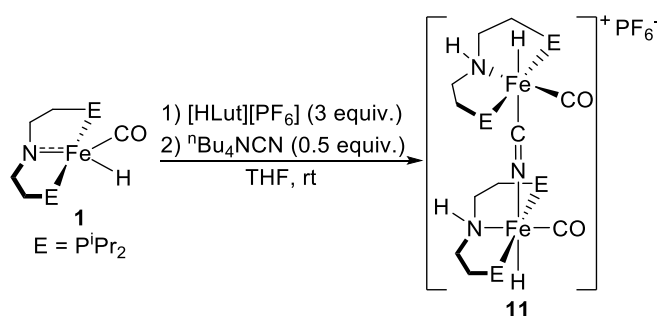


Figure 8: Calculated free energies of dimerization pathways that could lead to CO transfer between iron centers. All energies are in kcal/mol at 298K.

given that these reactions presumably proceed via dissociative ligand substitution followed by a relatively simple association between two iron centers, they are likely also kinetically feasible. Overall, based on our computational studies, we propose that the cationic, 16 e⁻ complex **5** is partially responsible for the formation of **4** during catalysis. There are three potential pathways for the formation of the cationic complex **5** in catalysis: a) Protonation of the dihydride complex **2** to form the dihydrogen complex **8**, which may be on-cycle in catalysis, followed by dissociation of the resultant dihydrogen ligand. b) Dissociation of an X-type ligand during catalysis, such as formate in formic acid dehydrogenation, or an alkoxide ligand in alcohol dehydrogenation. 3) Protonation of the amido complex **1** by an acid with a non-coordinating conjugate base, such as DBU-H⁺ (DBU = 1,8-Diazabicyclo5.4.0undec-7-ene) in CO₂ hydrogenation.^{18,46}

Dimeric Iron Complexes Supported by ^RPN^HP Ligands



Scheme 7: Synthesis of **11** from **1**.

There is currently only one example of a dimeric species supported by a ^RPN^HP ligand,²⁷ and it is not related to the dimeric intermediates proposed in the deactivation of **1** and related species. Further, species with an asymmetric end-on bridging CO ligand are also uncommon.⁴⁴ To provide indirect evidence that complexes of this type are plausible as intermediates in decomposition, we utilized a bridging ligand that is isoelectronic to CO, CN⁻. Addition of 0.5 equiv. of ⁿBu₄NCN to *in situ* generated **6** in THF at room temperature (Scheme 7) resulted in complete conversion to a single, asymmetric product with two inequivalent ³¹P NMR signals at 97.8 and 92.2 ppm and two inequivalent hydride resonances in the ¹H NMR spectrum at -13.7 and -20.8 ppm. We assigned this as the CN⁻ bridging complex [{(ⁱPrPN^HP)Fe(H)(CO)} {μ-CN}]⁺ (**11**), which was crystallized when the PF₆ anion was replaced with the BAr^F₄ anion (Figure 9). Single crystal X-ray diffraction shows that the two planes defined by P-N-P-Fe units are roughly parallel (at an angle of 8.5°), but that the N-Fe-Fe-N dihedral angle is 80°, so the pincer ligands are not aligned if the molecule is viewed down an axis comprising two iron centers. The N-H moieties on the two ⁱPrPN^HP ligands

are pointed towards each other and the iron centers. Both iron centers exhibit the standard distorted octahedral geometry observed with the $i\text{PrPN}^{\text{HP}}$ ligand, with P-Fe-P bond angles of $159.08(8)$ and $164.55(8)^\circ$, respectively. Additionally, the iron centers are pushed out of the P-N-P plane, toward the bridging CN^- ligand. One is 0.385 \AA and the other 0.257 \AA away from the P-N-P plane, indicating that the $i\text{PrPN}^{\text{HP}}$ ligands are bending downward and away from each other, which may be required due to steric reasons to accommodate dimerization. Overall, **11** is only the second example of a dimeric complex with a $i\text{PrPN}^{\text{HP}}$ ligand and confirms that it is possible to form a stable structure with a two-atom ligand bridging the iron centers.

To assess the synthetic feasibility of a complex with an asymmetric end-on bridging CO ligand, we next performed stoichiometric reactions between **6** and the proposed catalytic intermediates **1** and **10**. These complexes were selected as they are some of the only proposed catalytic intermediates related to **1** that are stable enough to readily isolate. No intermediates were detected in the reaction of **1** and **6** at room temperature and a small amount ($\sim 5\%$) of **4** and free $i\text{PrPN}^{\text{HP}}$ (along with a precipitate) were formed immediately. The amount of **4** and free $i\text{PrPN}^{\text{HP}}$ increased slowly over time, decomposing completely over the course of 4 days. In contrast, a reaction between **6** (or **5-THF**) and the formate complex **10** resulted in the rapid formation of two products

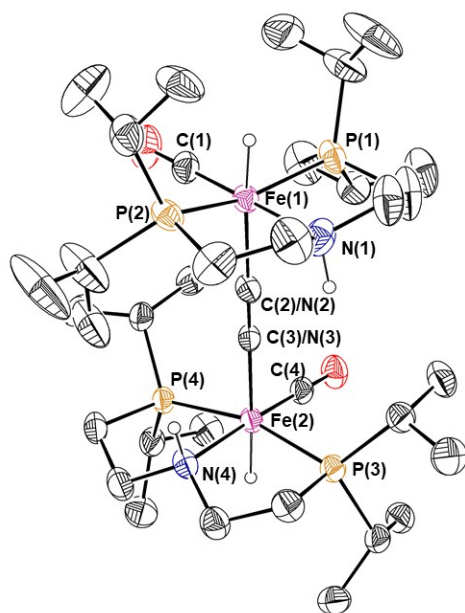


Figure 9: ORTEP of **11** with ellipsoids at 30% probability. Hydrogens not bound to Fe or N, solvent of crystallization, and BARF_4 anion omitted for clarity. Orientation of bridging CN ligand could not be unambiguously established and as a result the bridging ligand was modelled as a freely-refining 180° disordered CN bridge. Bond distances (\AA) and angles ($^\circ$): Fe(1)-N(1) 2.091(6), Fe(2)-N(4) 2.089(8), Fe(1)-C(1) 1.720(8), Fe(2)-C(4) 1.718(9), Fe(1)-P(1) 2.194(2), Fe(1)-P(2) 2.2001(19), Fe(2)-P(3) 2.196(2), Fe(2)-P(4) 2.197(2); P(1)-Fe(1)-P(2) $164.55(8)$, P(3)-Fe(2)-P(4) $159.08(8)$.

in a 10:1 ratio as determined by ^1H NMR spectroscopy (Scheme 8). The minor product is **4**.⁴⁷ The major product contains a resonance in the ^1H NMR spectrum at 8.23 ppm that integrates to 1 proton and a resonance at -25.66 ppm that integrates to two protons. We assign this complex as the symmetrical dimer [$\{(i^{\text{Pr}}\text{PN}^{\text{HP}})\text{Fe}(\text{H})(\text{CO})\}_2\{\mu\text{-OC}(\text{H})\text{O}\}^+$] (**12**, Scheme 8). Only one peak for **12** is observed in the ^{31}P NMR spectrum, consistent with this assignment. A solution state IR spectrum taken of **12** in C_6D_6 contains a strong band at 1900 cm^{-1} , corresponding to the carbonyl ligand stretch. An additional intense band is observed at 1588 cm^{-1} , which matches with carboxylate C–O stretching frequencies measured in previously studied κ^1, κ^1 -bridging formate complexes.⁴⁸ Compound **12** quickly decomposes upon exposure to vacuum, precluding isolation, but slow diffusion of pentane into the reaction mixture resulted in single crystals, which allowed us to confirm its structure (Figure 10). The geometry around both iron centers is distorted octahedral, with geometrical parameters similar to related monomeric species.²⁷ The iron centers in this dimer only lie 0.184 \AA and 0.123 \AA out of the P–N–P plane toward the bridging formate, suggesting that the pincer ligand does not need to bend as much to accommodate a 3-atom bridge as it does to accommodate a 2-atom bridge in **11**.

Selective labelling of the precursor **10** with ^{13}C in the formate ligand reveals the production of $^{13}\text{CO}_2$ *in situ* during the reaction between **6** and **10** to form **12**. A reaction of **6** and **10** in thawing C_6D_6 under 1 atm of CO_2 leads to very little formation of **4** even after 96 hours (<1% in the first hour). This supports the possibility that decarboxylation of the dimeric formate **12** is linked to decomposition. No inclusion of the labelled carbon center as a CO ligand is observed in any of the products by ^{13}C or ^{31}P NMR spectroscopy. Formation of **12** from **6** (or **5-THF**) and **10** occurs in minutes at ambient temperature and is much faster than the rate of decomposition of **6** (either by itself or with any other potential catalytic intermediate present), which occurs in hours. This, combined with the fact that both of the precursors (**10** and **5**, or here the synthetic analogue **6**) are present in catalysis,¹⁹ suggest that decomposition in formic acid dehydrogenation may be mediated by the dimerization of **10** and **5** via a bridging formate ligand, bringing two metal centers into close proximity prior to rapid, bimolecular decomposition.

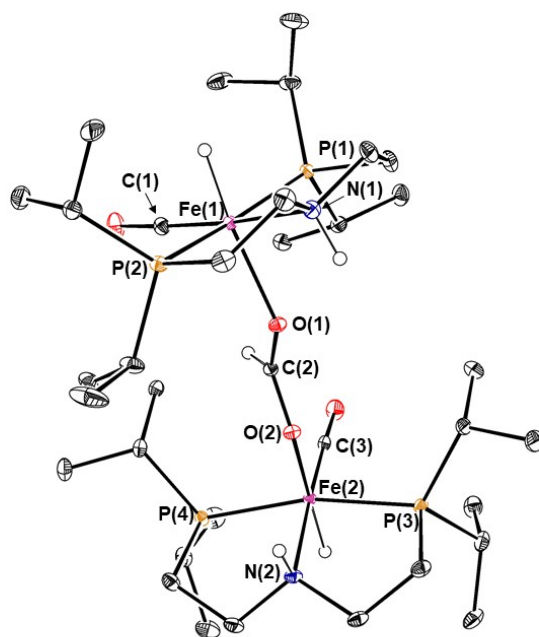
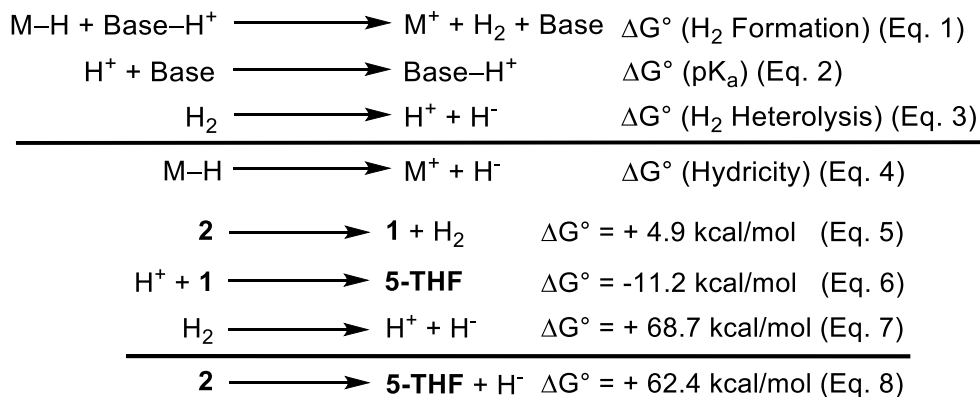


Figure 10: ORTEP of **12** with ellipsoids at 30% probability. Hydrogens not bound to Fe or N, solvent of crystallization, and PF_6^- anion omitted for clarity. Bond distances (Å) and angles ($^\circ$): Fe(1)-N(1) 2.0721(13), Fe(2)-N(2) 2.0723(15), Fe(1)-C(1) 1.7225(15), Fe(2)-C(3) 1.7231(15), Fe(1)-P(1) 2.2151(4), Fe(1)-P(2) 2.2148(4), Fe(2)-P(3) 2.2173(4), Fe(2)-P(4) 2.2261(4), Fe(1)-O(1) 2.0854(10), Fe(2)-O(2) 2.0746(10), O(1)-C(2) 1.2553(17), C(2)-O(2) 1.2546(17); P(1)-Fe(1)-P(2) 166.750(17), P(3)-Fe(2)-P(4) 168.318(17), Fe(1)-O(1)-C(2) 130.29(9), Fe(2)-O(2)-C(2) 129.64(9), O(1)-C(2)-O(2) 124.53(13).

*Determination of the Thermodynamic Hydricity of **2** and its Implications for Catalysis*

A consequence of our studies on deactivation of **1** and related species is that they provide a basis for us to determine the thermodynamic hydricity of the iron dihydride, ($i^{\text{Pr}}\text{PN}^{\text{H}}\text{P}$) $\text{Fe}(\text{H})_2(\text{CO})$ (**2**).

Understanding the thermodynamic hydricity of transition metal catalysts is important for designing new catalysts, as it provides information about the ability of a transition metal hydride to donate H⁻ to a substrate.⁴⁹ Here, this is valuable because compound **2** is a key species in hydrogenation reactions, where it is proposed to deliver H₂ to the substrate being reduced,^{13-14,15c,15d,16-18} as well in dehydrogenation reactions, where it is responsible for the liberation of H₂.^{13a,16,19-22} Specifically, the studies described above enable us to generate a thermodynamic cycle to measure hydricity based on the heterolysis of H₂.⁴⁹ In order to construct the cycle, knowledge is required about the following three free energies: a) The free energy of protonating the hydride with an acid to form H₂ (Eq. 1). b) The free energy of protonating the conjugate base of the acid used in Eq. 1 with a dissociated proton, determined by the pK_a of that acid (Eq. 2). c) The free energy of H₂ heterolysis in a given solvent, which is a thermodynamic constant (Eq. 3).^{49c} These can be combined using Hess' Law to determine the thermodynamic hydricity of a hydride (Eq. 4). Given that **1** contains an internal base and readily binds H₂ to form **2**, a modified version of this cycle can be used to determine the thermodynamic hydricity of **2** (Figure 11). One requirement for determining the thermodynamic hydricity of **2** is the pK_a of the N–H proton in **5-THF**. This was estimated to be 8.2 by titrating a solution of **1** with 2,6-lutidinium BAr^F₄ in THF,⁵⁰ which corresponds to a free energy of protonation of -11.2 kcal/mol. The thermodynamic cycle derived in Figure 11 and Equations 5-8, shows that with this pK_a the hydricity of **2** can be established if the binding constant of H₂ to **1** to form **2** is known. A van't Hoff plot obtained using variable-temperature ¹H NMR spectroscopy (288-333K, see SI for further details) of the equilibrium of **1** and H₂ and **2** indicates that ΔG° = -4.9 kcal/mol for this reaction. Combining these two values with the free energy of heterolysis of H₂^{49c} reveals that the hydricity of **2** is 62.4 ± 1.4 kcal/mol.⁵¹



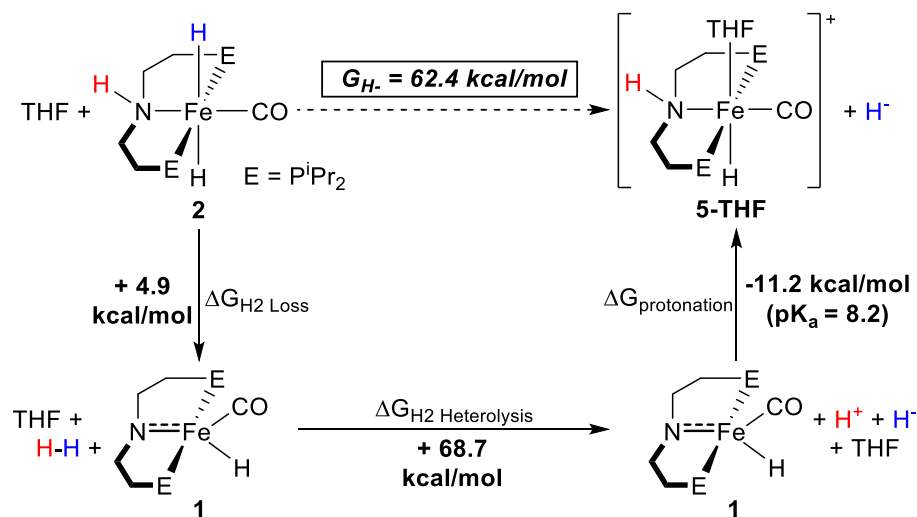
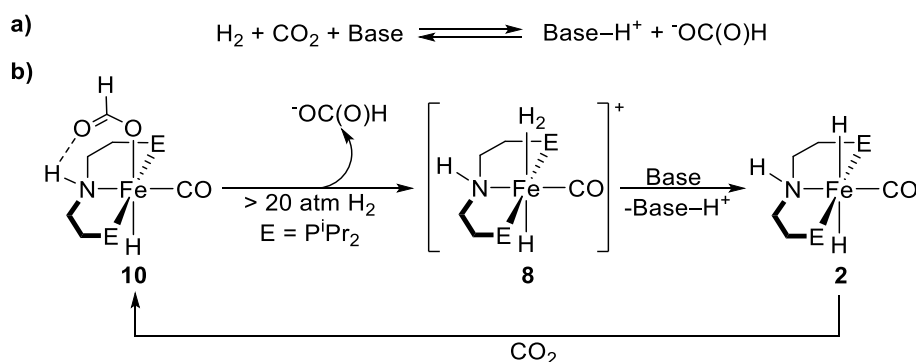


Figure 11: Thermodynamic cycle for experimentally determining the hydricity of **2**.

This is one of the first thermodynamic hydricities measured in THF, and only the second for a system that can activate H_2 via a pathway involving MLC. Complex **2** is a weaker hydride donor than the only other iron complex with a measured hydricity in THF, the cationic complex $[\text{Fe}(\text{SiP}_3)(\text{H}_2)(\text{H})]^+$ ($\text{SiP}_3 = \text{Si}(\textit{ortho}\text{-P}^i\text{Pr}_2\text{C}_6\text{H}_4)_3$), which has a hydricity of 54.0 kcal/mol.⁵² It is also a weaker hydride donor than the related ruthenium pincer complex $(^t\text{BuPN}_{\text{py}}\text{P})\text{Ru}(\text{H})_2(\text{CO})$ ($(^t\text{BuPN}_{\text{py}}\text{P} = (\text{CH}_2\text{P}^t\text{Bu}_2)_2\text{C}_5\text{H}_3\text{N})$), which has a hydricity in THF of 44.6 kcal/mol.⁵³ This is consistent with previous results, which show that heavier transition metals are more hydridic than their first row congeners,^{49c} although this interpretation is complicated by the fact that **2** is supported by a different pincer ligand than $(^t\text{BuPN}_{\text{py}}\text{P})\text{Ru}(\text{H})_2(\text{CO})$. In fact, the field would benefit from rigorous studies in THF (or a related organic solvent) exploring how thermodynamic hydricities vary as both ligand structure and the metal are systematically varied. Finally, the calculated thermodynamic hydricity of **2** suggests that it may be a weaker hydride donor than



Scheme 9: a) Overall reaction for reversible CO_2 hydrogenation in the presence of stoichiometric base and b) mechanism of catalysis showing the importance of base selection.

formate, which was reported to have a hydricity ≥ 42.7 kcal/mol in THF.⁵³ This means that **2** may only be able to insert CO₂ to form the formate complex **10** due to the free energy associated with binding the formate ligand to the iron, coupled with the thermodynamic stabilization gained by the formation of an N–H...O(formate) hydrogen bond (Scheme 9).^{19,21}

The hydricity of **2** also serves as a starting point for understanding its reactivity in catalysis. Relative to other complexes in THF, **2** appears to be a weak hydride donor and therefore **5** must be a very potent hydride acceptor. For dehydrogenative catalysis, this characteristic is valuable, and may help explain the high activity of **2** in reactions such as formic acid dehydrogenation, where **5** is directly invoked as the species responsible for abstracting a hydride from a formate anion (Figure 12).¹⁹ In a reaction such as CO₂ hydrogenation to formate, the hydricity of the active catalyst plays an important role in the choice of reaction conditions, particularly if reaction reversibility is desired (Scheme 9a).^{12,49b} Specifically, the choice of base is dependent upon the catalyst hydricity. This is because the base plays an important role in catalyst turnover (Scheme 9b). After CO₂ insertion into **2**, it is proposed that formate is displaced by H₂ to form the molecular hydrogen complex **8**. Regeneration of **2** takes place through the deprotonation of **8** by an equivalent of base. The strength of the base necessary to deprotonate H₂ in **8** to generate the metal hydride **2** is given by reorganizing the thermodynamic cycle established by Equations 1-4. This gives a pK_a of 8.2 for **8** (identical to the pK_a determined for the N–H of **5-THF**). The product of the overall reaction is [base–H⁺][[–]OC(O)H] (Scheme 9a). If the desire is to achieve a reversible system for hydrogenation of CO₂, H₂, and base to formate and the protonated base, then the best base is one which is strong enough to deprotonate **8**, but as weak as possible to ensure H₂ generation is possible in the reverse reaction (Scheme 9a, reverse reaction). In fact, a reversible system of the type could assist in the creation of a “hydrogen battery” based on formic acid and using H₂ instead of electrons.⁵⁴ The hydricity of **2** suggests that 2,6-lutidine, or a base whose conjugate acid has with

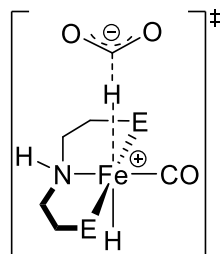


Figure 12: Transition state for hydride abstraction from a formate anion by **5**.

a similar pK_a (approximately 7 in water), should be strong enough to deprotonate **8** but allow the reaction to remain very close to thermoneutral, which allows for facile reaction reversibility.

The importance of thermodynamic hydricity, however, extends to catalysis that does not require stoichiometric base for turnover. The weak hydricity of **2** makes it necessary to utilize a strong acid to generate **8**. Current mechanistic proposals suggest that there are two cases where the molecular H_2 complex **8** is an intermediate in dehydrogenation reactions that involve **2** (Figure 13): a) When a dehydrogenative substrate is very acidic (*e.g.* formic acid), calculations predict it can directly protonate a hydride ligand of **2**,¹⁹ and b) When a protic substrate or reaction additive that is not a strong acid (*e.g.* a primary alcohol) is hydrogen-bonded to the N–H of the ligand, it is proposed to be acidic enough to directly protonate a hydride of **2**.^{13a,20b} The second instance has been invoked both as a “proton-shuttling” pathway, where more electron-poor, or more acidic, proton shuttles demonstrate higher activity, as well as in a directed ionic dehydrogenation mechanism.⁵⁵ For precatalyst design, these findings have several implications: a) Given that **2** is so poorly hydridic, very strong acids will continue to be necessary for direct protonation of the hydride; this is likely only possible for substrates such as formic acid. b) Protonation of **2** from an alcohol is only possible when the pendant amine ligand is a good hydrogen bond donor. If the N–H moiety is removed, and the substrate is not a strong acid such as formic acid, it must be replaced with another hydrogen bond donor either appended to the catalyst or in solution. Additionally, making the N–H of **2** more acidic may enhance activation of substrates which can act as a hydrogen bond acceptor.

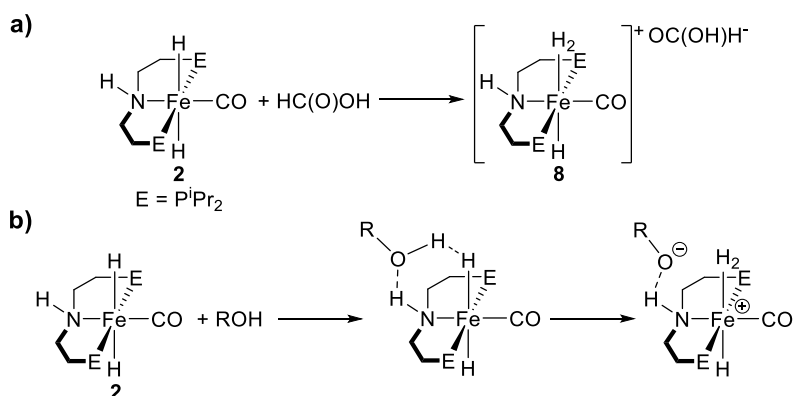
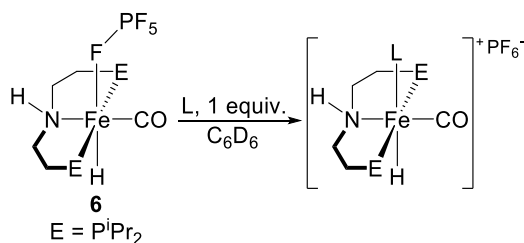


Figure 13: Proposed formation of dihydrogen complexes in dehydrogenation reactions using **2** for either **a)** highly acidic substrates such as formic acid or **b)** less acidic substrates such as alcohols.

Strategies for Improving Catalysis by Preventing Decomposition Due to **5**

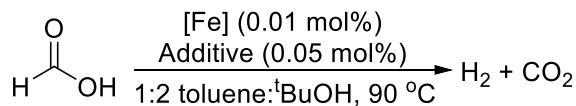
Given that **5** is likely responsible for catalyst decomposition, limiting either its formation or its ability to interact with other catalyst molecules could result in improvements in catalysis. Additionally, because **5** is on the catalytic cycle for some reactions, any strategy to prevent decomposition must allow **5** to remain thermodynamically and kinetically accessible in order for the catalyst to re-enter the productive cycle. In principle, this could be achieved through successful attachment of **2** or its derivatives to a supporting surface. We propose, however, to sequester **5** in catalysis through the addition of a simple L- or X-type ligand that can dissociate to access the cycle but will inhibit decomposition through dimerization. Stoichiometric reactions suggest that a variety of phosphine ligands, provided they are not too sterically bulky, can bind to **6** (Table 1) and form complexes of the type $[(^i\text{PrPN}^{\text{HP}})\text{Fe}(\text{H})(\text{CO})(\text{PR}_3)]^+$. Interestingly, no decomposition is observed when products of the reaction between **6** and small phosphines are allowed to stand in a solution of C_6D_6 at room temperature for four hours. This suggests that addition of small, simple L-type ligands that can reversibly bind could improve catalyst lifetime, as significant decomposition of **6** alone in solution is observed over this timeframe.



Ligand	Cone Angle (°)	Binds to 6
PMe_3	118	Yes
PEt_3	132	Yes
P^iPr_3	160	Yes*
PCy_3	179	No
P^tBu_3	182	No

Table 1: Binding of small, monodentate phosphine ligands to **6**. *The spectrum of this reaction remains broadened, but noticeably shifted. We interpret this as transient binding of P^iPr_3 to the iron center.

Guided by our stoichiometric results on phosphine binding to **6**, we endeavored to improve formic acid dehydrogenation using **1**, which is proposed to generate **8** *in situ*.^{19,26} This reaction is important because formic acid can be used as a source of H_2 in hydrogen storage, but at this stage the majority of base-metal catalysts capable of formic acid dehydrogenation only give significant activity in the presence of additives such as excess ligand, exogenous base, or a Lewis acid.⁵⁶ As shown in Table 2, **1** gives 1,300 TONs (13% conversion at 0.01 mol% catalyst loading) for additive-free formic acid dehydrogenation over 3 hours in a 1:2 toluene: $^t\text{BuOH}$ solvent mixture

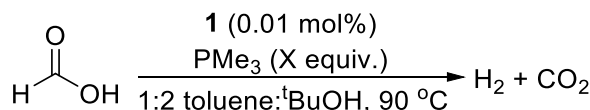


Entry	[Fe]	Additive	TON (1 h) ^a	TON (time) ^b	Yield (%)
1	1	None	1,100	1,300 (3 h)	13
2	1	PMe ₃	1,800	2,300 (8 h)	23
3	1	P ⁱ Pr ₃	1,700	1,800 (4 h)	18
4	1	P ^t Bu ₃	1,300	1,400 (3 h)	14
5	7	None	1,500	1,900 (8 h)	19
6	11^c	None	1,800	1,900 (3 h)	19

Table 2. Effect of simple monodentate phosphine additives on additive-free formic acid dehydrogenation using **1** and related precatalysts. Reaction conditions: Formic acid (110 μL , 2.91 mmol), Fe (0.01 mol%, 291 μL of a 1 mM stock solution in toluene), phosphine (0.05 mol%, if using, added as a 1% stock solution in toluene), 5.00 mL total reaction volume, 90 $^\circ\text{C}$. Turnover numbers (TON) were measured using a gas buret. ^aThis value is the TON after the first hour. ^bThis value is the maximum TON that was recorded. The time indicates how long it took for catalysis to stop and for the maximum TON to be obtained. Reported results are the average of two trials, errors \pm 10%. ^c0.005 mol% of **11** was used because there are two iron centers present in the complex.

(Entry 1).⁵⁷ However, addition of five equivalents of PMe₃ increases catalyst productivity by 75% and leads to a TON of 2,300 after 8 hours (Entry 2). Importantly, no CO, which could in principle poison the catalyst, was detected (see SI). This result suggests that PMe₃ stabilizes the catalyst, as predicted by the phosphine binding studies (Table 2). We next examined the effect of adding other monodentate phosphine ligands, including PⁱPr₃ (Table 2, Entry 3) and P^tBu₃ (Entry 4). The beneficial catalytic effects of the additive decrease with increasing phosphine cone angle, with the following order of improvement in TON observed: PMe₃ > PⁱPr₂ > P^tBu₃. In fact, P^tBu₃, which does not bind to the iron center in **6** (Table 2), does not lead to any improvement in TON within error. Complex **7**, [(ⁱPrPN^HP)Fe(H)(CO)(PMe₃)]⁺, which already has one equivalent of PMe₃ bound to the iron center, achieves a TON of 1,900 after 8 hours (Entry 5) without the addition of any excess PMe₃. This indicates that even one equivalent of PMe₃ gives improved catalyst lifetime and productivity compared to **1**. Finally, we utilized the CN-bridged dimer **11** as a precatalyst, to investigate the effect of the additional steric bulk provided by the second iron center on the proposed catalyst decomposition. Compound **11** gives a TON of 1,900 after 3 hours (assuming that both iron centers are catalytically active, Entry 6), a 45% improvement compared to **1**. However, it is clear that rapid catalyst death remains an issue, as **11** has a TON after 1 hour of 1,700, indicating that 94% of the total TONs are achieved in the first hour of catalysis, compared with 78% for **1** and 5 equivalents of PMe₃.

We next investigated the effect of varying the number of equivalents of the best additive, PMe₃ (Table 3). Halving the equivalents added to 2.5 relative to **1** gives 2,000 turnovers in 4 hours (Entry



Entry	Equiv. PMe ₃	TON (1 h) ^a	TON (time) ^b	Yield (%)
1	0	1,100	1,300 (3 h)	13
2	2.5	1,800	2,000 (4 h)	20
3	5	1,800	2,300 (8 h)	23
4	10	1,700	2,000 (8 h)	20

Table 3. Formic acid dehydrogenation using **1** and varying equivalents of PMe₃. Reaction conditions: Formic acid (110 μL , 2.91 mmol), **1** (0.01 mol%, 291 μL of a 1 mM stock solution in toluene), PMe₃ (added as a 1 vol% stock solution in toluene, equivalents given relative to **1**), 5.00 mL total reaction volume, 90 $^\circ\text{C}$. Turnover numbers (TON) were measured using a gas buret. ^aThis value is the TON after the first hour. ^bThis value is the maximum TON that was recorded. The time indicates how long it took for catalysis to stop and for the maximum TON to be obtained. Reported results are the average of two trials, errors \pm 10%.

2), whereas doubling the equivalents to 10 results in 2,000 turnovers over 8 hours (Entry 4). From these results, we conclude that 5 equivalents of PMe₃ relative to **1** is the optimal combination to extend catalyst lifetime and achieve the highest possible TON. To further understand the effect of PMe₃, we performed kinetic analyses on the catalytic activity of **1** alone, as well as with 5 equivalents of PMe₃ (Figure 14). The difference is striking, with the trial with PMe₃ added rapidly outpacing the trial with **1** alone from the first timepoint taken after 10 minutes. Given that we propose that PMe₃ assists in catalysis by stabilizing the catalyst, rather than generating a more active catalytic species, these data suggest that catalyst decomposition begins immediately upon initiating catalysis. Unfortunately, for technical reasons it is not possible to obtain earlier data points, which may indicate that **1** is initially more active, but rapidly deactivates compared to **1** with PMe₃ present. We were, however, able to study catalyst decomposition in the presence and absence of PMe₃ in a J. Young NMR tube under conditions directly comparable to catalysis (see SI). These studies indicate that as has been observed previously,²⁶ the major catalyst decomposition product is $[(^i\text{PrPN}^{\text{H}}\text{P})\text{Fe}(\text{H})(\text{CO})_2]^+$ (**4**) (along with free ligand). Consistent with our hypotheses, in the reaction with 5 equivalents of PMe₃ a significantly smaller amount of **4** is formed after one hour, suggesting that excess PMe₃ inhibits catalyst decomposition. In reactions with PMe₃, **7** can be detected by NMR spectroscopy. Given that the coordinatively unsaturated intermediate that is likely stabilized by the presence of PMe₃ is proposed to be present in many other catalytic reactions involving **1**, we hypothesize that our simple strategy for improving catalyst productivity will be relevant to many other reactions apart from formic acid dehydrogenation. Further, it was recently reported that the presence of phosphine additives can stabilize Ru-MACHO for ester

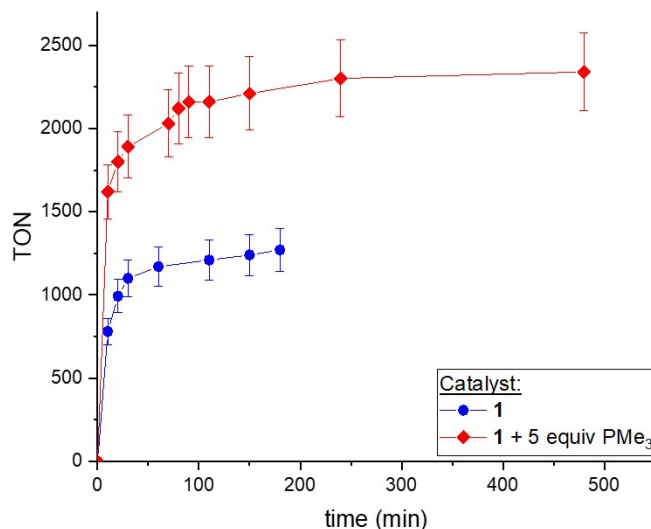


Figure 14. Kinetic traces for formic acid dehydrogenation using **1** (blue circles) and **1** with 5 equiv PMe_3 (red diamonds). No time points were collected once catalytic turnover had stopped. Error bars $\pm 10\%$.

hydrogenation.⁵⁸ The exact reasons for the increased productivity observed in the presence of phosphine ligands was not elucidated, but our results may also explain the improvements in the analogous ruthenium system.

Conclusions

The decomposition of catalysts related to $(i\text{PrPNP})\text{Fe}(\text{H})(\text{CO})$ (**1**) and $(i\text{PrPN}^{\text{HP}})\text{Fe}(\text{H})_2(\text{CO})$ (**2**) has prevented their widespread use as replacements for precious metal catalysts in hydrogenation and dehydrogenation reactions. It has also limited their effectiveness in new catalytic reactions. This work provides valuable insight into the decomposition pathways of **1** and **2** in catalysis by studying the reactivity of several key catalytic intermediates which had not previously been observed. In particular, we have characterized the unstable complexes $[(i\text{PrPN}^{\text{HP}})\text{Fe}(\text{H})(\text{CO})(\text{L})]^+$ (**5-L**; solv = THF or N_2) and $[(i\text{PrPN}^{\text{HP}})\text{Fe}(\text{H})(\text{H}_2)(\text{CO})]^+$ (**8**). Complex **8**, which can be prepared by the addition of H_2 to $(i\text{PrPN}^{\text{HP}})\text{Fe}(\text{H})(\text{CO})(\text{PF}_6)$ (**6**), is a rare example of an iron-containing species with a H_2 ligand that has been characterized by neutron diffraction. Our results indicate that **5** and related complexes decompose via a bimolecular pathway, and we have isolated rare examples of dimeric iron complexes ligated by $i\text{PrPN}^{\text{HP}}$ ligands. Finally, we have used our results to develop an improved system for formic acid dehydrogenation using **1** and intend to continue to use the fundamental insight from this work, including the measurement of the thermodynamic hydricity of $(i\text{PrPN}^{\text{HP}})\text{Fe}(\text{H})_2(\text{CO})$ (**2**), to develop improved RPN^{HP} ligated catalysts in the future.

Acknowledgements

N.H. and W.H.B. acknowledge support from the U.S. Department of Energy, Office of Science, Basic Energy Sciences, Catalysis Science Program, under Award DE-SC0018222. T.M.T. thanks the NSF for support as an NSF Graduate Research Fellow. The work at BNL (M.Z.E.) was supported by the U.S. Department of Energy (DOE), Office of Science, Office of Basic Energy Sciences, Division of Chemical Sciences, Geosciences & Biosciences, under Contract No. DE-SC0012704. Computational work was supported by the facilities and staff of the Yale University Faculty of Arts and Sciences High Performance Computing Center. A portion of this research used resources at the Spallation Neutron Source, specifically the TOPAZ beamline, a DOE Office of Science User Facility operated by the Oak Ridge National Laboratory. We thank Dr. Adam Pearce and Jeremy Weber for valuable assistance in obtaining IR spectra.

Supporting Information

Experimental and computational procedures, characterization data, NMR spectra, and other details are available via the Internet at <https://pubs.acs.org/>.

Competing Financial Interests

The authors declare no competing financial interests.

References

1. The standard definition of metal-ligand cooperation (MLC) is that both the metal and the ligand are directly involved in the bond activation process. For more information see: Khusnutdinova, J. R.; Milstein, D. Metal–Ligand Cooperation. *Angew. Chem. Int. Ed.* **2015**, *54*, 12236-12273.
2. (a) Szabó, K. J.; Wendt, O. F. *Pincer and Pincer-Type Complexes: Applications in Organic Synthesis and Catalysis*; John Wiley & Sons, Inc.: Weinheim, Germany, 2014; (b) Gunanathan, C.; Milstein, D. Bond Activation and Catalysis by Ruthenium Pincer Complexes. *Chem. Rev.* **2014**, *114*, 12024-12087; (c) Werkmeister, S.; Neumann, J.; Junge, K.; Beller, M. Pincer-Type Complexes for Catalytic (De)Hydrogenation and Transfer (De)Hydrogenation Reactions: Recent Progress. *Chem. Eur. J.* **2015**, *21*, 12226-12250; (d) Morales-Morales, D. *Pincer Compounds: Chemistry and Applications*; Elsevier: Amsterdam, Netherlands, 2018; (e) Valdés, H.; García-Eleno, M. A.; Canseco-Gonzalez, D.; Morales-Morales, D. Recent Advances in Catalysis with Transition-Metal Pincer Compounds. *ChemCatChem* **2018**, *10*, 3136-3172.
3. Clarke, Z. E.; Maragh, P. T.; Dasgupta, T. P.; Gusev, D. G.; Lough, A. J.; Abdur-Rashid, K. A Family of Active Iridium Catalysts for Transfer Hydrogenation of Ketones. *Organometallics* **2006**, *25*, 4113-4117.
4. Mukherjee, A.; Srimani, D.; Ben-David, Y.; Milstein, D. Low-Pressure Hydrogenation of Nitriles to Primary Amines Catalyzed by Ruthenium Pincer Complexes. Scope and mechanism. *ChemCatChem* **2017**, *9*, 559-563.
5. Zhang, J.; Leitus, G.; Ben-David, Y.; Milstein, D. Efficient Homogeneous Catalytic Hydrogenation of Esters to Alcohols. *Angew. Chem. Int. Ed.* **2006**, *45*, 1113-1115.
6. Sánchez, P.; Hernández-Juárez, M.; Rendón, N.; López-Serrano, J.; Santos, L. L.; Álvarez, E.; Paneque, M.; Suárez, A. Hydrogenation/Dehydrogenation of N-Heterocycles Catalyzed by Ruthenium Complexes Based on Multimodal Proton-Responsive CNN(H) Pincer Ligands. *Dalton Trans.* **2020**, *49*, 9583-9587.
7. Tanaka, R.; Yamashita, M.; Nozaki, K. Catalytic Hydrogenation of Carbon Dioxide Using Ir(III)–Pincer Complexes. *J. Am. Chem. Soc.* **2009**, *131*, 14168-14169.

8. Kuriyama, W.; Matsumoto, T.; Ogata, O.; Ino, Y.; Aoki, K.; Tanaka, S.; Ishida, K.; Kobayashi, T.; Sayo, N.; Saito, T. Catalytic Hydrogenation of Esters. Development of an Efficient Catalyst and Processes for Synthesising (R)-1,2-Propanediol and 2-(1-Methoxy)ethanol. *Org. Proc. Res. Develop.* **2012**, *16*, 166-171.
9. Zhang, J.; Leitus, G.; Ben-David, Y.; Milstein, D. Facile Conversion of Alcohols into Esters and Dihydrogen Catalyzed by New Ruthenium Complexes. *J. Am. Chem. Soc.* **2005**, *127*, 10840-10841.
10. Egorova, K. S.; Ananikov, V. P. Toxicity of Metal Compounds: Knowledge and Myths. *Organometallics* **2017**, *36*, 4071-4090.
11. (a) Garbe, M.; Junge, K.; Beller, M. Homogeneous Catalysis by Manganese-Based Pincer Complexes. *Eur. J. Org. Chem.* **2017**, *2017*, 4344-4362; (b) Alig, L.; Fritz, M.; Schneider, S. First-Row Transition Metal (De)Hydrogenation Catalysis Based On Functional Pincer Ligands. *Chem. Rev.* **2019**, *119*, 2681-2751; (c) Junge, K.; Papa, V.; Beller, M. Cobalt-Pincer Complexes in Catalysis. *Chem. Eur. J.* **2019**, *25*, 122-143.
12. Bernskoetter, W. H.; Hazari, N. Reversible Hydrogenation of Carbon Dioxide to Formic Acid and Methanol: Lewis Acid Enhancement of Base Metal Catalysts. *Acc. Chem. Res.* **2017**, *50*, 1049-1058.
13. (a) Chakraborty, S.; Lagaditis, P. O.; Forster, M.; Bielinski, E. A.; Hazari, N.; Holthausen, M. C.; Jones, W. D.; Schneider, S. Well-Defined Iron Catalysts for the Acceptorless Reversible Dehydrogenation-Hydrogenation of Alcohols and Ketones. *ACS Catal.* **2014**, *4*, 3994-4003; (b) Werkmeister, S.; Junge, K.; Wendt, B.; Alberico, E.; Jiao, H.; Baumann, W.; Junge, H.; Gallou, F.; Beller, M. Hydrogenation of Esters to Alcohols with a Well-Defined Iron Complex. *Angew. Chem. Int. Ed.* **2014**, *53*, 8722-8726; (c) Elangovan, S.; Wendt, B.; Topf, C.; Bachmann, S.; Scalone, M.; Spannenberg, A.; Jiao, H.; Baumann, W.; Junge, K.; Beller, M. Improved Second Generation Iron Pincer Complexes for Effective Ester Hydrogenation. *Adv. Synth. Catal.* **2016**, *358*, 820-825.
14. Bornschein, C.; Werkmeister, S.; Wendt, B.; Jiao, H.; Alberico, E.; Baumann, W.; Junge, H.; Junge, K.; Beller, M. Mild and Selective Hydrogenation of Aromatic and Aliphatic (di)nitriles with a Well-Defined Iron Pincer Complex. *Nat. Commun.* **2014**, *5*, 4111.
15. (a) Rezayee, N. M.; Samblanet, D. C.; Sanford, M. S. Iron-Catalyzed Hydrogenation of Amides to Alcohols and Amines. *ACS Catal.* **2016**, *6*, 6377-6383; (b) Schneck, F.; Assmann, M.; Balmer, M.; Harms, K.; Langer, R. Selective Hydrogenation of Amides to Amines and Alcohols Catalyzed by Improved Iron Pincer Complexes. *Organometallics* **2016**, *35*, 1931-1943; (c) Jayarathne, U.; Zhang, Y.; Hazari, N.; Bernskoetter, W. H. Selective Iron-Catalyzed Deaminative Hydrogenation of Amides. *Organometallics* **2017**, *36*, 409-416; (d) Lane, E. M.; Zhang, Y.; Hazari, N.; Bernskoetter, W. H. Sequential Hydrogenation of CO₂ to Methanol Using a Pincer Iron Catalyst. *Organometallics* **2019**, *38*, 3084-3091.
16. Chakraborty, S.; Brennessel, W. W.; Jones, W. D. A Molecular Iron Catalyst for the Acceptorless Dehydrogenation and Hydrogenation of N-Heterocycles. *J. Am. Chem. Soc.* **2014**, *136*, 8564-8567.
17. Xu, R.; Chakraborty, S.; Bellows, S. M.; Yuan, H.; Cundari, T. R.; Jones, W. D. Iron-Catalyzed Homogeneous Hydrogenation of Alkenes under Mild Conditions by a Stepwise, Bifunctional Mechanism. *ACS Catal.* **2016**, *6*, 2127-2135.
18. Zhang, Y.; MacIntosh, A. D.; Wong, J. L.; Bielinski, E. A.; Williard, P. G.; Mercado, B. Q.; Hazari, N.; Bernskoetter, W. H. Iron Catalyzed CO₂ Hydrogenation to Formate Enhanced by Lewis Acid Co-Catalysts. *Chem. Sci.* **2015**, *6*, 4291-4299.
19. Bielinski, E. A.; Lagaditis, P. O.; Zhang, Y.; Mercado, B. Q.; Würtele, C.; Bernskoetter, W. H.; Hazari, N.; Schneider, S. Lewis Acid-Assisted Formic Acid Dehydrogenation Using a Pincer-Supported Iron Catalyst. *J. Am. Chem. Soc.* **2014**, *136*, 10234-10237.
20. (a) Alberico, E.; Sponholz, P.; Cordes, C.; Nielsen, M.; Drexler, H.-J.; Baumann, W.; Junge, H.; Beller, M. Selective Hydrogen Production from Methanol with a Defined Iron Pincer Catalyst under Mild Conditions. *Angew. Chem. Int. Ed.* **2013**, *52*, 14162-14166; (b) Bielinski, E. A.; Förster, M.; Zhang, Y.; Bernskoetter, W. H.; Hazari, N.; Holthausen, M. C. Base-Free Methanol Dehydrogenation Using a Pincer-Supported Iron Compound and Lewis Acid Co-catalyst. *ACS Catal.* **2015**, *5*, 2404-2415.
21. Sharninghausen, L. S.; Mercado, B. Q.; Crabtree, R. H.; Hazari, N. Selective Conversion of Glycerol to Lactic Acid with Iron Pincer Precatalysts. *Chem. Commun.* **2015**, *51*, 16201-16204.
22. Glüer, A.; Foerster, M.; Celinski, V. R.; Schmedt auf der Guenne, J.; Holthausen, M. C.; Schneider, S. Highly Active Iron Catalyst for Ammonia Borane Dehydrocoupling at Room Temperature. *ACS Catal.* **2015**, *5*, 7214-7217.
23. Pena-Lopez, M.; Neumann, H.; Beller, M. Iron(II) Pincer-Catalyzed Synthesis of Lactones and Lactams through a Versatile Dehydrogenative Domino Sequence. *ChemCatChem* **2015**, *7*, 865-871.
24. Lane, E. M.; Uttley, K. B.; Hazari, N.; Bernskoetter, W. Iron-Catalyzed Amide Formation from the Dehydrogenative Coupling of Alcohols and Secondary Amines. *Organometallics* **2017**, *36*, 2020-2025.
25. Lane, E. M.; Hazari, N.; Bernskoetter, W. H. Iron-Catalyzed Urea Synthesis: Dehydrogenative Coupling of Methanol and Amines. *Chem. Sci.* **2018**, *9*, 4003-4008.

26. Curley, J. B.; Bernskoetter, W. H.; Hazari, N. Additive-Free Formic Acid Dehydrogenation Using a Pincer-Supported Iron Catalyst. *ChemCatChem* **2020**, *12*, 1934-1938.
27. Koehne, I.; Schmeier, T. J.; Bielinski, E. A.; Pan, C. J.; Lagaditis, P. O.; Bernskoetter, W. H.; Takase, M. K.; Wurtele, C.; Hazari, N.; Schneider, S. Synthesis and Structure of Six-Coordinate Iron Borohydride Complexes Supported by PNP Ligands. *Inorg. Chem.* **2014**, *53*, 2133-2143.
28. A search of the Cambridge Structural Database (Version 5.41) for transition metal complexes with bound PF₆ ligands resulted in 49 examples of crystallographically characterized complexes.
29. Honeychuck, R. V.; Hersh, W. H. Coordination of "Noncoordinating" Anions: Synthesis, Characterization, and X-Ray Crystal Structures of Fluorine-Bridged Hexafluoroantimonate(1-), Tetrafluoroborate(1-), and Hexafluorophosphate(1-) Adducts of [R₃P(CO)₃(NO)W]⁺. An Unconventional Order of Anion Donor Strength. *Inorg. Chem.* **1989**, *28*, 2869-2886.
30. Brookhart, M.; Grant, B.; Volpe, A. F. [(3,5-(CF₃)₂C₆H₃)₄B][H(OEt)₂]⁺: A Convenient Reagent for Generation and Stabilization of Cationic, Highly Electrophilic Organometallic Complexes. *Organometallics* **1992**, *11*, 3920-3922.
31. DFT indicates that three bands would be expected in this region, which are caused by combinations of the N≡N, C≡O, and Fe-H vibrations. However, the vibration primarily associated with the Fe-H vibration is predicted to be weak in intensity and is therefore unlikely to be observed experimentally.
32. The most likely cause of isomers is related to the orientation of a ligand coordinated to iron with respect to the N-H group of the pincer. This can result in *syn* and *anti* isomers, as described for complex **7**.
33. On another occasion when we crystallized **5-N₂**, it co-crystallized with a molecule of [(ⁱPrPN^HP)Fe(H)(CO)(OH₂)]⁺ (**5-H₂O**) in the unit cell. We believe that the presence of **5-H₂O** was caused by adventitious water and this is discussed further in the SI. This includes characterization of **5-H₂O** by ¹H and ³¹P NMR spectroscopy.
34. Hazari, N. Homogeneous Iron Complexes for the Conversion of Dinitrogen into Ammonia and Hydrazine. *Chem. Soc. Rev.* **2010**, *39*, 4044-4056.
35. Greif, A. H.; Hrobárik, P.; Kaupp, M. Insights into trans-Ligand and Spin-Orbit Effects on Electronic Structure and Ligand NMR Shifts in Transition-Metal Complexes. *Chem. Eur. J.* **2017**, *23*, 9790-9803.
36. Alvarez, S. Coordinating Ability of Anions, Solvents, Amino Acids, and Gases towards Alkaline and Alkaline-Earth Elements, Transition Metals, and Lanthanides. *Chem. Eur. J.* **2020**, *26*, 4350-4377.
37. Bootsma, A. N.; Wheeler, S. Popular Integration Grids Can Result in Large Errors in DFT-Computed Free Energies. *ChemRxiv* **2019**, 8864204, v5.
38. Although the reported decomposition product in this paper is the dicarbonyl, **3**, in the presence of excess formic acid the dicarbonyl **3** is protonated to form **4**. For additional information about protonation of iron(0) PNP complexes at the metal center, see ref. 26.
39. Morris, R. H. Dihydrogen, Dihydride and in Between: NMR and Structural Properties of Iron Group Complexes. *Coord. Chem. Rev.* **2008**, *252*, 2381-2394.
40. (a) Gorgas, N.; Alves, L. G.; Stöger, B.; Martins, A. M.; Veiros, L. F.; Kirchner, K. Stable, Yet Highly Reactive Nonclassical Iron(II) Polyhydride Pincer Complexes: Z-Selective Dimerization and Hydroboration of Terminal Alkynes. *J. Am. Chem. Soc.* **2017**, *139*, 8130-8133; (b) Gorgas, N.; Brünig, J.; Stöger, B.; Vanicek, S.; Tilset, M.; Veiros, L. F.; Kirchner, K. Efficient Z-Selective Semihydrogenation of Internal Alkynes Catalyzed by Cationic Iron(II) Hydride Complexes. *J. Am. Chem. Soc.* **2019**, *141*, 17452-17458.
41. Although it was possible to generate crystals of **8** for single crystal X-ray and neutron diffraction studies, we were not able to fully characterize **8**. This is because **8** needs to be stored under an atmosphere of H₂, and exposure of the compound to vacuum in both solution or the solid-state causes loss of the H₂ ligand. In the single crystal experiments, when **8** was removed from the H₂ atmosphere, it was immediately immersed in oil and placed under a liquid N₂ cold stream, which significantly reduces the rate of decomposition.
42. (a) Ricci, J. S.; Koetzle, T. F.; Bautista, M. T.; Hofstede, T. M.; Morris, R. H.; Sawyer, J. F. Single-Crystal X-Ray and Neutron Diffraction Studies of an η₂-Dihydrogen Transition-Metal Complex: *trans*-[Fe(η₂-H₂)(H)(PPh₂CH₂CH₂PPh₂)₂]BPh₄. *J. Am. Chem. Soc.* **1989**, *111*, 8823-8827; (b) Van der Sluys, L. S.; Eckert, J.; Eisenstein, O.; Hall, J. H.; Huffman, J. C.; Jackson, S. A.; Koetzle, T. F.; Kubas, G. J.; Vergamini, P. J.; Caulton, K. G. An Attractive cis-Effect of Hydride on Neighbor Ligands: Experimental and Theoretical Studies on the Structure and Intramolecular Rearrangements of Fe(H)₂(η₂-H₂)(PEtPh₂)₃. *J. Am. Chem. Soc.* **1990**, *112*, 4831-4841.
43. (a) Moodley, K. G.; Engel, D. W.; Field, J. S.; Haines, R. J. Synthesis and Protonation of Mixed Diphosphorus Ligand-Bridged Derivatives of Di-Iron Nonacarbonyl. *Polyhedron* **1993**, *12*, 533-542; (b) Shade, J. E.; Pearson, W. H.; Brown, J. E.; Bitterwolf, T. E. Photochemical Reimer-Tiemann Reactions of (η⁵-C₅H₅)₂Fe₂(μ-CO)₂(μ-Ph₂PCH₂PPh₂) and (η⁵-C₅H₅)₂Fe₂(μ-CO)₂(μ-Ph₂PCH₂CH₂PPh₂). The Molecular Structures of (η⁵-C₅H₅)₂Fe₂(μ-

CO)₂(μ-Ph₂PCH₂CH₂PPh₂) and (η⁵-CHOC₅H₄)(η⁵-C₅H₅)Fe₂(μ-CO)₂(μ-Ph₂PCH₂CH₂PPh₂). *Organometallics* **1995**, *14*, 157-161; (c) Ellermann, J.; Gabold, P.; Knoch, F. A.; Moll, M.; Pohl, D.; Sutter, J.; Bauer, W. Chemie Polyfunktioneller Moleküle CXXII. Das Komplexchemische Verhalten von Bis(diphenylphosphino)amin Gegenüber Dieisennonacarbonyl und Reaktionen von [Fe₂(CO)₆(μ-CO)(μ-Ph₂P-NH-PPh₂)] · THF. *J. Organomet. Chem.* **1996**, *525*, 89-107; (d) Lu, C. C.; Saouma, C. T.; Day, M. W.; Peters, J. C. Fe(I)-Mediated Reductive Cleavage and Coupling of CO₂: An FeII(μ-O,μ-CO)FeII Core. *J. Am. Chem. Soc.* **2007**, *129*, 4-5; (e) Braunschweig, H.; Dewhurst, R. D.; Schneider, C. Steric Control between Neutral Metal-Only Lewis Pairs and Metal-Stabilized Gallenium and Gallium Cations. *Organometallics* **2016**, *35*, 1002-1007.

44. (a) Zhang, Z.-Z.; Zhang, J.-K.; Zhang, W.-D.; Xi, H.-P.; Cheng, H.; Wang, H.-G. Carbonylation of Iron(II) Halide in the Presence of Chelate Diphosphine Ligands. Molecular Structure of a Novel Intermolecular Adduct [FeC₁₂(dppe)₂][Fe₂(CO)₂Cl₄]. *J. Organomet. Chem.* **1996**, *515*, 1-9; (b) Monillas, W. H.; Yap, G. P. A.; MacAdams, L. A.; Theopold, K. H. Binding and Activation of Small Molecules by Three-Coordinate Cr(I). *J. Am. Chem. Soc.* **2007**, *129*, 8090-8091; (c) Femoni, C.; Iapalucci, M. C.; Longoni, G.; Zacchini, S. The Chemistry of Hydridocarbonylferrates Revisited: Syntheses and Structures of the New [H₂Fe₄(CO)₁₂]²⁻ and [HFe₅(CO)₁₄]³⁻ anions, and the [Fe(DMF)₄][Fe₄(CO)₁₂(μ⁵-η²-CO)(μ-H)₂] Adduct Containing an Unprecedented Isocarbonyl. *Dalton Transactions* **2011**, *40*, 8685-8694; (d) Akturk, E. S.; Yap, G. P. A.; Theopold, K. H. Mechanism-Based Design of Labile Precursors for Chromium(I) Chemistry. *Chem. Commun.* **2015**, *51*, 15402-15405.

45. We propose that the dimerization of **5** and **9** is more thermodynamically favorable than the dimerization of **5** and **2** or **5** and **10** due to the instability of **9**, rather than any stabilization of the dimeric product. Specifically, whereas **2** and **10** are relatively stable complexes, **9** readily loses MeOH via 1,2-elimination under ambient conditions, see reference 20b.

46. Although there is evidence that DBU can coordinate to some transition metal complexes (see for example: Sole, R. D.; Luca, A. D.; Mele, G.; Vasapollo, G. First Evidence of Formation of Stable DBU Zn-Phthalocyanine Complexes: Synthesis and Characterization. *J. Porphyr. Phthalocyanines* **2005**, *9*, 519-527), there is no evidence that it can coordinate to **1** and related complexes used for CO₂ hydrogenation.

47. It is notable that the NMR spectra from these reactions do not show any free ligand. The free ligand that needs to be formed to balance the stoichiometry associated with forming **4** is presumably either in the form of a paramagnetic complex or broadened by transient binding to other metal centers.

48. Deacon, G. B.; Phillips, R. J. Relationships Between the Carbon-Oxygen Stretching Frequencies of Carboxylato Complexes and the Type of Carboxylate Coordination. *Coord. Chem. Rev.* **1980**, *33*, 227-250.

49. (a) Wiedner, E. S.; Chambers, M. B.; Pitman, C. L.; Bullock, R. M.; Miller, A. J. M.; Appel, A. M. Thermodynamic Hydricity of Transition Metal Hydrides. *Chem. Rev.* **2016**, *116*, 8655-8692; (b) Ceballos, B. M.; Yang, J. Y. Directing the Reactivity of Metal Hydrides for Selective CO₂ Reduction. *Proc. Natl. Acad. Sci. U. S. A.* **2018**, *115*, 12686-12691; (c) Brereton, K. R.; Smith, N. E.; Hazari, N.; Miller, A. J. M. Thermodynamic and Kinetic Hydricity of Transition Metal Hydrides. *Chem. Soc. Rev.* **2020**, *49*, 7929-7948.

50. Using the method described in *J. Org. Chem.* **2002**, *67*, 1873-1881, the relative pK_a of **5** was determined to be -0.48 pK_a units, corresponding to a K_{eq} of 3.0. See the SI for more experimental details and the UV-Vis spectra used in the K_{eq} determination.

51. This is the value assuming that the product of protonating **1** with 2,6-lutidinium BA_{TF}⁻ is **5-THF**, as convention dictates that solvent binding after hydride transfer is assumed in hydricity measurements. However, from our earlier results we know that **5-THF** is in equilibrium with **5-N₂**, although **5-THF** is favored. Given this equilibrium, N₂ binding cannot have a large effect on the equilibrium constant used to determine the pK_a of **5-THF**. The error in this measurement would imply an error in the hydricity of **2** of less than 1 kcal/mol, less than the error already accounted for in the measurement.

52. Fong, H.; Peters, J. C. Hydricity of an Fe-H Species and Catalytic CO₂ Hydrogenation. *Inorg. Chem.* **2015**, *54*, 5124-5135.

53. Mathis, C. L.; Geary, J.; Ardon, Y.; Reese, M. S.; Philliber, M. A.; VanderLinden, R. T.; Saouma, C. T. Thermodynamic Analysis of Metal-Ligand Cooperativity of PNP Ru Complexes: Implications for CO₂ Hydrogenation to Methanol and Catalyst Inhibition. *J. Am. Chem. Soc.* **2019**, *141*, 14317-14328.

54. Boddien, A.; Federsel, C.; Sponholz, P.; Mellmann, D.; Jackstell, R.; Junge, H.; Laurenczy, G.; Beller, M. Towards the Development of a Hydrogen Battery. *Energy Environ. Sci.* **2012**, *5*, 8907-8911.

55. (a) Dub, P. A.; Gordon, J. C. Metal-Ligand Bifunctional Catalysis: The “Accepted” Mechanism, the Issue of Concertedness, and the Function of the Ligand in Catalytic Cycles Involving Hydrogen Atoms. *ACS Catal.* **2017**, *7*, 6635-6655; (b) Smith, N. E.; Bernskoetter, W. H.; Hazari, N. The Role of Proton Shuttles in the Reversible Activation of Hydrogen via Metal-Ligand Cooperation. *J. Am. Chem. Soc.* **2019**, *141*, 17350-17360.

56. Sordakis, K.; Tang, C.; Vogt, L. K.; Junge, H.; Dyson, P. J.; Beller, M.; Laurenczy, G. Homogeneous Catalysis for Sustainable Hydrogen Storage in Formic Acid and Alcohols. *Chem. Rev.* **2018**, *118*, 372-433.
57. Reactions were compared at low conversions of formic acid because trends in catalyst performance are easier to identify under these conditions. It is possible to obtain higher conversions of formic acid at higher catalyst loadings.
58. Tindall, D. J.; Menche, M.; Schelwies, M.; Paciello, R. A.; Schäfer, A.; Comba, P.; Rominger, F.; Hashmi, A. S. K.; Schaub, T. Ru⁰ or Ru^I: A Study on Stabilizing the “Activated” Form of Ru-PNP Complexes with Additional Phosphine Ligands in Alcohol Dehydrogenation and Ester Hydrogenation. *Inorg. Chem.* **2020**, *59*, 5099-5115.

TOC Graphic

Ubiquitous Base-Metal (De)hydrogenation Catalyst:

